The influence of source heterogeneity on the U–Th–Pa–Ra disequilibria in post-glacial tholeiites from Iceland

J.M. Koornneef [a,*], A. Stracke [a,1], B. Bourdon [a,2], K. Grönvold [b]

[a] Institute of Geochemistry and Petrology, ETH Zürich, Clausiusstrasse 25, 8092, Switzerland
[b] Nordic Volcanological Institute, University of Iceland, Sturlugata 7, 101 Reykjavik, Iceland

Abstract

We investigate the relative influence of mantle upwelling velocity and source heterogeneity on the melting rates recorded by ^{230}Th–^{238}U, ^{231}Pa–^{235}U and ^{226}Ra–^{230}Th disequilibria in post-glacial tholeiites from Iceland's main rift areas. The measured (^{230}Th/^{238}U) ratios range from 1.085 to 1.247, the (^{231}Pa/^{235}U) ratios from 1.333 to 1.925, and the (^{226}Ra/^{230}Th) ratios from 0.801 to 1.218. A general positive correlation between ^{230}Th excesses and distance from the inferred plume centre is consistent with a model of decreasing mantle upwelling velocity with increasing distance from the plume axis. However, the model is not substantiated by the (^{231}Pa/^{235}U) data as the correlation with distance from the plume centre is weak. On the scale of individual eruption centres, the observed U-series are influenced by variations in melt transport time, source porosity, and local variations in mantle upwelling velocity. Broad correlations between (^{230}Th/^{238}U) and (^{231}Pa/^{235}U) and highly incompatible trace element ratios for samples from the Western Volcanic Zone provide, however, evidence for a significant underlying effect of source heterogeneity on the U-series data. Low ^{230}Th and ^{231}Pa excesses in enriched samples from the Western Volcanic Zone with high U/Th, Nb/U and Nb/La indicate that partial melts from an enriched source component, characterised by high melt productivity but low bulk D_U/D_{Th}, influence the U-series systematics of the erupted melts. These results re-affirm the presence of comparatively larger abundances of enriched material in the mantle source beneath the South Western Rift of Iceland, which has been suggested based on relationships between highly incompatible element and Pb isotope ratios in Icelandic basalts. Overall, our results highlight the importance of lithological heterogeneity on the melting behaviour of the upper mantle and the composition of oceanic basalts.
© 2012 Elsevier Ltd. All rights reserved.

1. INTRODUCTION

Uranium series disequilibria in young oceanic basalts provide constraints on the dynamics of partial melting and melt extraction processes in the upper mantle. Specifically, they reveal information about mantle upwelling velocity, melt extraction rate, and residual porosity, but also about intrinsic properties of the mantle source such as its modal mineralogy and melt productivity (e.g., Condomines et al., 1981; Williams and Gill, 1989; McKenzie, 1985; Cohen and O'Nions, 1993; Iwamori, 1993; Spiegelman and Elliott, 1993; Turner et al., 1997; Bourdon et al., 1998, 2005, 2006; Sims et al., 1999; Stracke et al., 1999, 2006, 2003a; Peate et al., 2001; Kokfelt et al., 2003; Lundstrom et al., 2003; Pietruszka et al., 2009; Prytulak and Elliott, 2009).

During partial melting of the upper mantle, differences in residence time of the parent and daughter nuclides in the melt and residual solid mantle cause U-series disequilibrium. Proposed melting models range from 'dynamic melting' assuming rapid melt extraction with no equilibration between the partial melts and solid (McKenzie, 1985) to

---

* Corresponding author. Present address: Department of Petrology, Vrije Universiteit Amsterdam, de Boelelaan 1085, 1081 HV, The Netherlands. Tel.: +31 20 59 83725.
E-mail address: janne.koornneef@falw.vu.nl (J.M. Koornneef).
[1] Present address: Institut für Mineralogie, Westfälische Wilhelms Universität, 48149 Münster, Germany.
[2] Present address: Laboratoire de Géologie de Lyon, Ecole Normale Supérieure de Lyon, UCBL and CNRS, Lyon, France.

'equilibrium porous-flow' with continuous melt–solid equilibration (Spiegelman and Elliott, 1993). More complex models suggest a so-called two-porosity regime during melt extraction, which implies different degrees of melt–solid equilibration at different depths in the mantle (Iwamori, 1994; Lundstrom et al., 2000; Lundstrom, 2001; Jull et al., 2002). These melting models can be used to explain the observed U-series isotope variation by variation in mantle upwelling velocity, which is directly proportional to the melting rate, and residual porosity during partial melting. Generally, the above-mentioned models make the simplifying assumption that the mantle source has a homogeneous mineralogical composition. The presence of lithological heterogeneity in the mantle, however, may change its melting behaviour, because different lithologies have different modal composition, trace element partitioning characteristics, and melt productivity (Lundstrom et al., 1995; Bourdon et al., 1996; Hirschmann and Stolper, 1996; Stracke et al., 1999, 2003a; Pertermann and Hirschmann, 2003, 2004; Prytulak and Elliott, 2007, 2009).

Melt productivity for example – defined as the amount of melt formed per increment of pressure release – is consistently larger for mafic lithologies compared to peridotites (Hirschmann and Stolper, 1996; Asimow et al., 1997, 2001; Hirschmann et al., 1999a; Kogiso et al., 2004; Pertermann and Hirschmann, 2003) resulting in higher melting rates. Prytulak and Elliott (2009) pointed out that the differences in melt productivity and thus melting rate between peridotitic and pyroxenitic mantle components could have a much larger effect on the U-series nuclides in ocean island basalts (OIB) than differences in mantle upwelling velocity. Russo et al. (2009) suggested that melting of fertile pyroxenite veins could explain the relationships between trace element ratios and ^{230}Th and ^{226}Ra excesses observed in mid ocean ridge basalts (MORB) from the South-East Indian Ridge. The quantitative effect of lithological source heterogeneity on the U-series disequilibria, however, remains difficult to predict due to the uncertainty attached to the relevant melting and partitioning behaviour of lithologically different sources (e.g., Stracke et al., 1999; Bourdon and Sims, 2003).

In Icelandic rocks, correlations between major elements and trace element ratios and long-lived isotopes suggest that melting of at least two components, one isotopically depleted and one isotopically enriched, is required to explain the observed trends (Wood, 1981; Elliott et al., 1991; Maclennan et al., 2003; Stracke et al., 2003b; Kokfelt et al., 2006; Maclennan, 2008a; Stracke and Bourdon, 2009; Peate et al., 2010; Koornneef et al., 2012). Although the nature of the enriched Icelandic source component remains controversial, most previous studies favoured ancient recycled oceanic crust, present in form of small-scale mafic components (e.g., Chauvel and Hémond, 2000; Skovgaard et al., 2001; Stracke et al., 2003b; Kokfelt et al., 2006; Peate et al., 2010). Enrichments in Nb/La and Nb/U ratios combined with higher ^{206}Pb/^{204}Pb in samples from the Western Rift Zone and the Reykjanes Peninsula suggest that the abundance of this enriched component is larger beneath these main rift areas compared to the Northern Rift Zone (Hanan et al., 2000; Koornneef et al., 2012). The inferred lithological source heterogeneity may therefore affect the

U-series disequilibria in young Icelandic lavas. Kokfelt et al., 2003, however, mainly attributed the observed differences in (^{230}Th/^{238}U) (where parentheses denote activity ratios) in Icelandic rift-zone lavas to variations in mantle upwelling rate as a result of decreasing mantle potential temperature away from the plume centre (Kokfelt et al., 2003; Bourdon et al., 2006).

Here, we present new ^{226}Ra–^{230}Th–^{238}U and ^{231}Pa–^{235}U disequilibria data on 25 geochemically well characterised post-glacial tholeiites from Iceland's main rift areas (Koornneef et al., 2012) and replicate analyses of four lavas from Theistareykir previously analysed by Stracke et al. (2006, 2003a). In addition to ^{230}Th–^{238}U disequilibria, the aim is to use (^{231}Pa/^{235}U) ratios, which are more sensitive to variability in melting rates compared to (^{230}Th/^{238}U) ratios, to evaluate the potential effects of source heterogeneity and the inferred variations in regional upwelling velocity on the U-series disequilibria.

Even though variations in mantle potential temperature have no resolvable influence on the major, trace element, and long-lived isotope systematics (Koornneef et al., 2012), our (^{230}Th/^{238}U) data demonstrate that systematic variation in regional mantle upwelling velocity across Iceland is required (Kokfelt et al., 2006; Bourdon et al., 2006). Variability of the (^{230}Th/^{238}U) and (^{231}Pa/^{235}U) ratios on a local scale and the observed correlations with highly incompatible trace elements reveal an important role of source heterogeneity for establishing the U-series disequilibria in Icelandic rift zone lavas.

2. SAMPLE PREPARATION AND ANALYTICAL TECHNIQUES

U, Th, Pa and Ra concentrations and isotope ratios were determined on 25 post glacial tholeiites from Iceland's main rift areas (Fig. 1). Koornneef et al. (2012) previously reported their major and trace element and Hf and Nd isotope composition. In addition to the samples from the Reykjanes Peninsula (RP, $n = 10$), the Western Volcanic Zone (WV, $n = 7$), and the Northern Volcanic Zone (NV, $n = 8$), we re-analysed four samples from Theistareykir, a small area in the Northern Volcanic Zone, that were previously analysed by Stracke et al. (2003a, 2006) for their U, Th, Pa and Ra concentrations and isotope ratios. Generally, the investigated samples are younger than 3000 years, with the exception of WV21 ($\sim$5300 years) and WV25 ($\sim$3400 years) and the Theistareykir samples, whose ages range between 3000 and 12,000 years (Table 1).

A detailed description of the chemical separation and measurement procedures is given in Koornneef et al. (2010, 2012). Approximately 1 g of sample powder was spiked with ^{236}U, ^{229}Th, ^{233}Pa and ^{228}Ra tracers and dissolved in a mixture of HF and HNO$_3$. After drying down, samples were re-dissolved in HCl and boric acid was used to remove fluorides. After conversion to a nitrate form, samples were loaded on a first 5 ml TRU-spec column yielding fractions of Ra + matrix, U + Pa and Th. In a second column step, U was separated from Pa on a 1 ml AG50-X8 column and the Th fraction was purified on a 0.2 ml AG1-X4 column. The Ra + matrix fraction from the first column
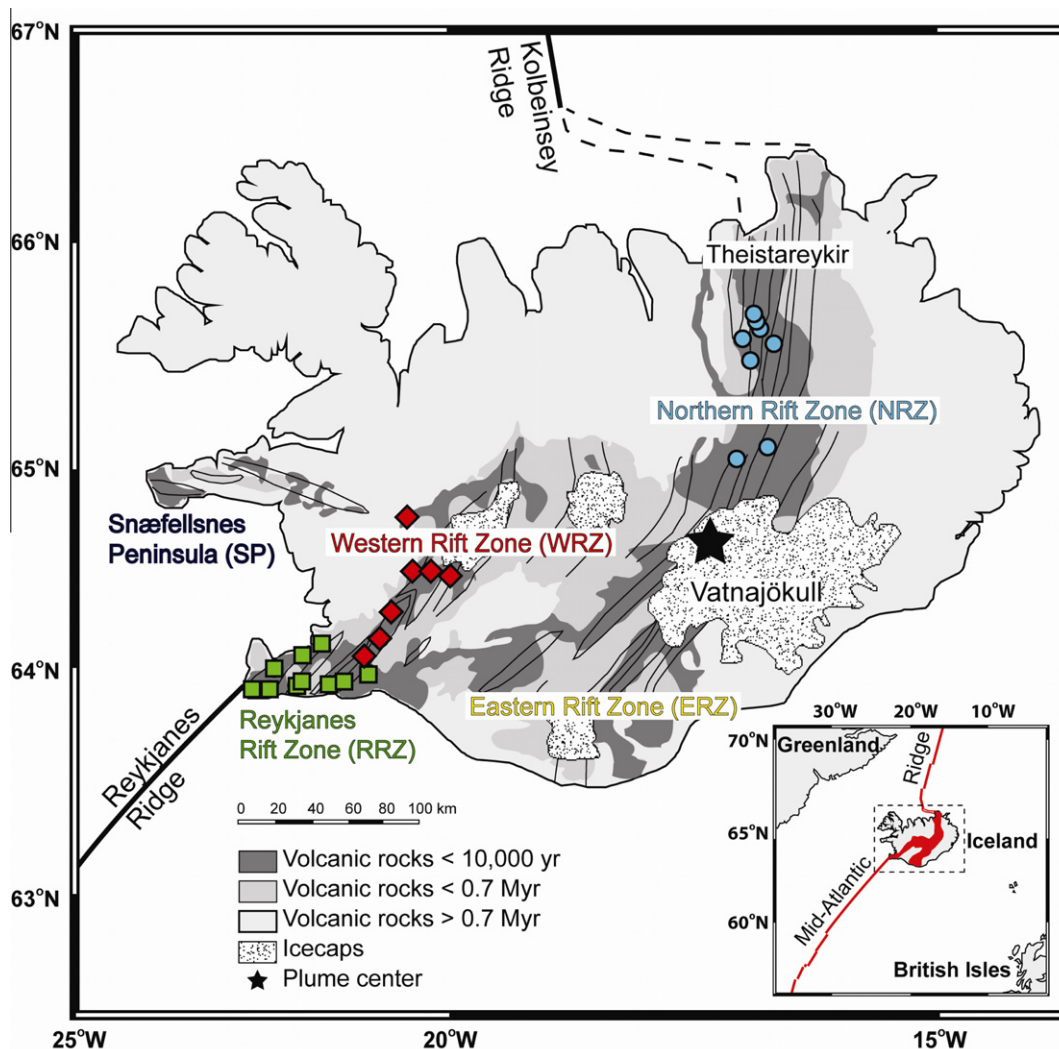
Fig. 1. Simplified geological map of Iceland showing the sampling localities of all 25 lavas (modified after geological map published on www.tephrabase.org). Green squares: Reykjanes Peninsula (RP); red diamonds: Western Volcanics (WV); blue cirkels: Northern Volcanics (NV); All samples are younger than 10,000 yr. (For interpretation of the references to colour in this figure legend, the reader is referred to the web version of this article.)

was further purified sequentially using a 20 ml and a 3 ml AG50-X8 column and a final 1 ml Sr-Spec column (Chabaux et al., 1994; Claude-Ivanaj et al., 1998). All U, Th, Pa and Ra concentrations and isotope ratios were determined by multi collector inductively coupled plasma mass spectrometry (MC-ICPMS) at ETH Zürich on a NU Plasma instrument. Sample reproducibility was evaluated by repeated measurements of USGS rock reference materials BCR-2 and W-2a and of rock standard TML, which were processed and measured contemporaneously with the samples and are reported in Koornneef et al. (2010).

3. RESULTS

U–Th–Pa and Ra concentrations and ^{230}Th–^{238}U, ^{231}Pa–^{235}U and ^{226}Ra–^{230}Th disequilibria data are presented in Table 1 and Figs. 2–4. Data corrected for post-eruptive decay (Table 1), which is mainly relevant for the

^{226}Ra-disequilibria of the lavas, are also shown in Fig. 3. Note that the accuracy of the age-corrected data is limited by the precision of the available age estimates for each lava flow (Peate et al., 2009; Sinton et al., 2005).

3.1. ^{238}U–^{234}U–^{230}Th disequilibria

High temperature processes do not significantly fractionate ^{234}U and ^{238}U isotopes. However, modern seawater has (^{234}U/^{238}U) > 1 (Chen et al., 1986), rendering the (^{234}U/^{238}U) ratios in oceanic basalts susceptible to disturbance by seawater–rock interaction. All RP, WV and NV samples have (^{234}U/^{238}U) within error of secular equilibrium, demonstrating they were not affected by post-eruptive seawater alteration. Samples from Theistareykir, however, have (^{234}U/^{238}U) ≠ 1, indicating they are affected by seawater alteration. The U-series systematics of these samples will be discussed in detail in Section 3.4.

Table 1
U–Th–Pa–Ra data on Icelandic postglacial main rift lavas.

Sample	Flow	Long. Lat.	Age[a,b] (years)	Distance[c] (km)	U (µg/g)	Th (µg/g)	Pa (fg/g)	Ra (fg/g)	$(^{234}U/^{238}U)$[d]	2SE (10^{-3})	$(^{238}U/^{232}Th)$	2SE (10^{-3})
RP1	Illahraun	21.99164.054	784	226	0.163	0.515	90.8	78.1	1.003	3	0.962	7
RP2	Afstaparhraun	22.17364.016	684	236	0.133	0.423	73.3	58.7	1.003	4	0.951	6
RP5	Stamparhraun	22.70963.830	784	268	0.126	0.393	67.9	50.3	0.999	3	0.973	5
RP6	Eldvarpahraun	22.60063.822	784	263	0.126		68.8	51.7	1.003	4		
					0.126	0.385	69.0	49.5	1.002	3	0.991	4
RP9	Arnarsetur	22.42663.890	784	253	0.175	0.534	110.0	77.7	1.004	1	0.992	8
RP10	Ögmundarhraun	22.23363.854	784	246	0.133	0.419	73.8	58.1	1.002	0	0.963	7
RP11	Herdísarvik	21.78663.870		225	0.117	0.361	68.4	49.0	1.001	4	0.985	5
RP12	Grindaskörð	21.74163.876	1049	223	0.165	0.512	89.0	79.8	1.003	1	0.978	8
RP15	Nesjahraun	21.44563.956	1800	206	0.145	0.454	80.8	62.3	1.005	0	0.967	4
RP56	Ögmundarhraun	22.15563.859	1009	242	0.132	0.409	73.5	59.2	1.002	2	0.981	8
WV16	Svínahraunsbruni	21.45264.028	840	203	0.172	0.533	89.4	75.6	0.999	3	0.982	4
WV18	Skjaldbreiður I	20.92064.437		165	0.068	0.205	39.4	25.7	1.002	4	1.010	5
WV20	Skjaldbreiður II	20.78364.444		159	0.142	0.445	75.8	57.8	0.994	3	0.971	7
WV21	Sköflungur	20.65064.447	5300	152	0.123	0.378	60.4	46.1	1.001	2	0.991	7
WV25	Thjófahraun	21.05164.263	3360	176	0.192	0.590	98.4	74.7	1.003	4	0.985	8
					0.191	0.593	97.8	74.9	1.002	3	0.980	3
WV27	Nesjahraun	21.24764.124	1800	190	0.142	0.443	83.3	52.2	0.999	3	0.973	4
WV31	Hallmundarhraun	20.84264.745	1050	159	0.090	0.290	56.8		0.999	3	0.945	4
					0.091	0.289	58.5	47.4	0.994	7	0.960	4
NV41	Prengslaborgir	16.94865.575	3000	104	0.148	0.479	66.9	60.8	1.000	0	0.936	4
NV42	Elda	16.94565.656	282	129	0.227	0.722	112.7	97.0	1.004	4	0.955	7
					0.227	0.728	116.9	94.8	1.001	4	0.946	3
NV45	Krafla	16.78465.718	282	121	0.225	0.718	111.4	96.3	1.007	3	0.950	8
NV48	Daleldar	16.79365.664	3000	116	0.228	0.723	114.9	96.0	1.000	3	0.957	7
NV49	Krafla	16.84165.795	27	129	0.164	0.526	85.2	74.5	1.001	0	0.946	7
NV50	Krafla	16.84165.795	27	129	0.165	0.542	100.3	67.2	0.999	4	0.924	9
NV52	Askja	16.72165.044	91	56	0.432		200.6	181.1	1.002	4		
					0.431	1.435	196.6	179.5	1.001	3	0.912	4
NV54	Frambruni	17.07565.017	649	44	0.193	0.642	84.9	81.6	1.001	2	0.914	3
9309	Theistareykir		8750	132	0.028	0.084	19.1	9.4	1.039	4	1.007	3
9383	Theistareykir		2850	141	0.059	0.188	33.1	24.5	1.006	4	0.953	3
9389	Theistareykir		11,250	141	0.030	0.094	16.3	10.9	1.035	4	0.960	3
9390	Theistareykir		11,250	142	0.006	0.017	3.5	0.0	1.099	8	1.012	2

Table 1 (*continued*)

Sample	(^{230}Th/^{232}Th)	2SE (10^{-3})	(^{230}Th/^{238}U)	2SE (10^{-3})	(^{231}Pa/^{235}U)	2SE (10^{-3})	(^{226}Ra/^{230}Th)	2SE (10^{-3})	(^{230}Th/^{238}U)$_i$[e]	(^{231}Pa/^{235}U)$_i$	(^{226}Ra/^{230}Th)$_i$
RP1	1.136	9	1.181	10	1.686	19	1.180	11	1.182	1.697	1.251
RP2	1.154	8	1.213	10	1.680	23	1.062	13	1.214	1.690	1.083
RP5	1.135	9	1.167	9	1.635	23	0.995	9	1.168	1.645	
RP6					1.662	13				1.673	
	1.108	10	1.118	10	1.668	14	1.026	8	1.119	1.679	1.036
RP9	1.153	11	1.162	12	1.911	37	1.114	14	1.163	1.926	1.160
RP10	1.147	9	1.191	10	1.684	19	1.067	13	1.192	1.696	1.094
RP11	1.162	9	1.180	9	1.773	17	1.032	10			
RP12	1.154	12	1.179	13	1.636	12	1.193	14	1.181	1.650	1.301
RP15	1.140	12	1.179	9	1.695	17	1.065	11	1.182	1.722	1.140
RP56	1.151	11	1.174	12	1.687	19	1.102	13	1.175	1.702	1.156
WV16	1.139	8	1.160	8	1.575	23	1.101	8	1.161	1.585	1.144
WV18	1.163	8	1.152	9	1.750	23	0.952	10			
WV20	1.108	9	1.140	11	1.618	18	1.038	12			
WV21	1.081	9	1.091	11	1.487	19	0.991	12	1.095	1.545	
WV25	1.070	10	1.087	12	1.558	12	1.044	10	1.088	1.595	1.193
	1.070	9	1.092	9	1.551	15	1.043	7	1.095	1.594	1.196
WV27	1.144	7	1.176	7	1.781	20	0.909	8	1.179	1.811	
WV31	1.185	8	1.254	8	1.906	29			1.256	1.927	
	1.190	11	1.240	10	1.943	17	1.218	8	1.242	1.964	1.341
NV41	1.069	9	1.142	9	1.378	21	1.051	9	1.146	1.403	1.183
NV42	1.098	8	1.149	11	1.506	14	1.080	12	1.150	1.509	1.090
	1.094	10	1.156	10	1.565	15	1.052	7	1.157	1.568	1.052
NV45	1.092	8	1.150	11	1.506	17	1.085	12	1.151	1.509	1.095
NV48	1.098	7	1.146	10	1.531	24	1.069	11	1.150	1.566	1.248
NV49	1.110	9	1.174	10	1.580	17	1.125	13	1.174	1.580	1.126
NV50	1.061	14	1.148	16	1.845	16	1.032	12	1.148	1.845	1.032
NV52					1.410	31				1.411	
	1.036	11	1.136	11	1.384	11	1.067	8	1.136	1.385	1.069
NV54	1.032	7	1.130	8	1.333	30	1.087	11	1.131	1.337	1.115
9309	1.228	11	1.220	9	2.068	37	0.801	6	1.238	2.285	
9383	1.168	10	1.225	9	1.701	43	0.985	7	1.231	1.745	
9389	1.153	11	1.201	10	1.670	24	0.887	6	1.223	1.850	
9390	1.101	13	1.089	12	1.877	13			1.098	2.112	

[a] Ages are from Peate et al. (2009) and Sinton et al. (2005), and from historical records (Askja and Krafla).

[b] Ages for Theistareykir samples represent the mean of the range reported in Stracke et al., 2003a.

[c] Distance from the plume centre calculated using the sampling coordinates relative to coordinates 64.5 °N, 17.3°W (Kokfelt et al., 2003).

[d] Activity ratios are calculated using: $\lambda_{234} = 2.8263 \times 10^{-6}$ yr^{-1}, $\lambda_{235} = 9.8485 \times 10$–$10$ yr^{-1}, $\lambda_{238} = 1.5513 \times 10^{-10}$ yr^{-1}, $\lambda_{232} = 4.9475 \times 10^{-11}$ yr^{-1}, $\lambda_{230} = 9.1577 \times 10^{-6}$ yr^{-1}, $\lambda_{231} = 2.1158 \times 10^{-5}$ yr^{-1}, $\lambda_{226} = 4.3322 \times 10^{-4}$ yr^{-1}.

[e] Initial activity ratios corrected for post eruptive decay. Note that for samples that have Ra-deficits no decay correction is given because it is unclear when and by what process the deficits were formed.
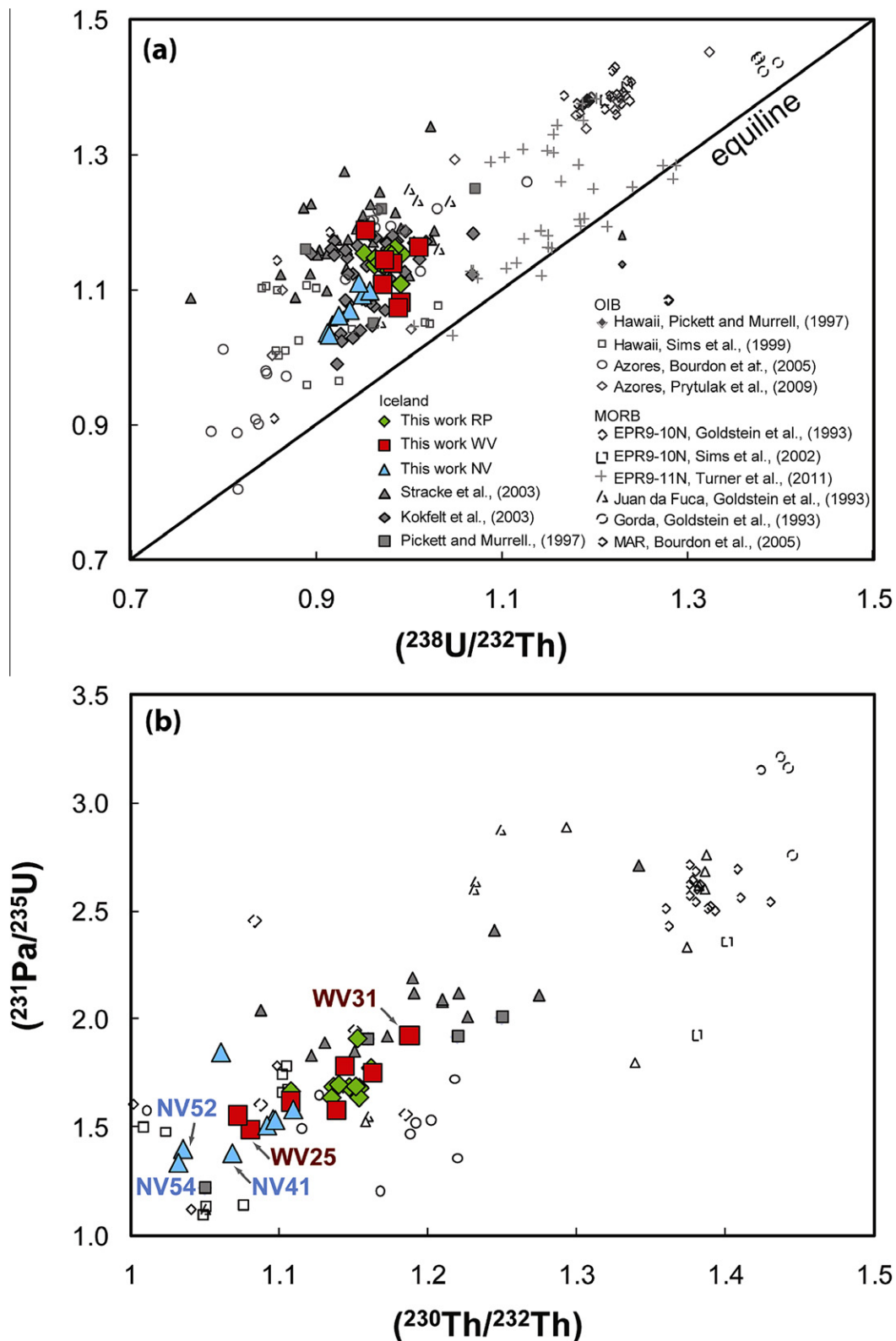
Fig. 2. (a) U–Th equiline diagram showing Icelandic data from this study compared to OIB and MORB literature data (see legend for references). (b) Diagram of (^{230}Th/^{232}Th) versus (^{231}Pa/^{235}U). Note the good correlation for Icelandic samples as opposed to the lack of correlation for other OIB and MORB localities.

All measured samples have ^{230}Th excesses (i.e., (^{230}Th/^{238}U) > 1) in agreement with previous studies on samples from the Icelandic rift zones (Peate et al., 2001; Kokfelt et al., 2003; Stracke et al., 2003a). Western Volca-
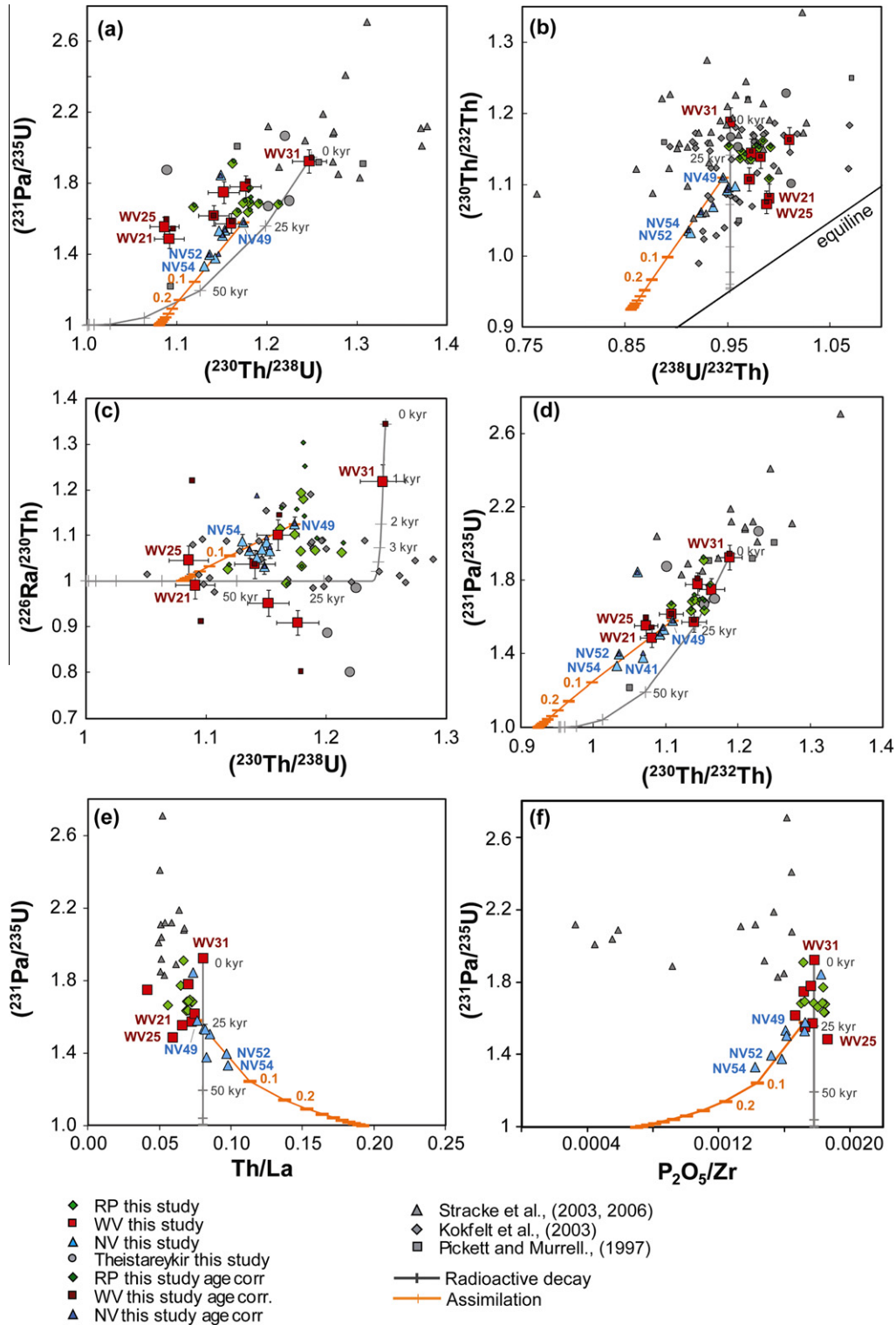
Fig. 3. Diagrams of (a) $(^{230}Th/^{238}U)$ versus $(^{231}Pa/^{235}U)$, (b) $(^{230}Th/^{232}Th)$ versus $(^{238}U/^{232}Th)$, (c) $(^{226}Ra/^{230}Th)$ versus $(^{230}Th/^{238}U)$, and (d) $(^{231}Pa/^{235}U)$ versus $(^{230}Th/^{232}Th)$ for samples from Iceland. Age corrected data (small symbols) are shown for samples with a known age. The effect of radioactive decay is illustrated by a trajectory (grey) calculated for sample WV31, the sample with highest ^{230}Th, ^{231}Pa and ^{226}Ra excesses measured in this study. Note the good correlation for Iceland data in diagram (d) as opposed to the less systematic variation in (a) and non-systematic variability in (c). For samples analysed multiple times (Table 1) the average is plotted in the figures. Error bars for WV samples represent 2σ standard deviations determined on multiple analyses of several rock standards digestions (Koornneef et al., 2010). For clarity these are only shown for WV samples. Orange model trends represent assimilation of sample NV49 by bulk binary mixing with a rhyolite (Kuritani et al. (2011) sample ID2405, Th = 7.11 ppm and Th/U of 3.54) assumed to be in secular equilibrium for $(^{231}Pa/^{235}U)$ and $(^{226}Ra/^{230}Th)$ and to have a $(^{230}Th/^{238}U) = 1.08$. Samples discussed specifically in the text are labelled.
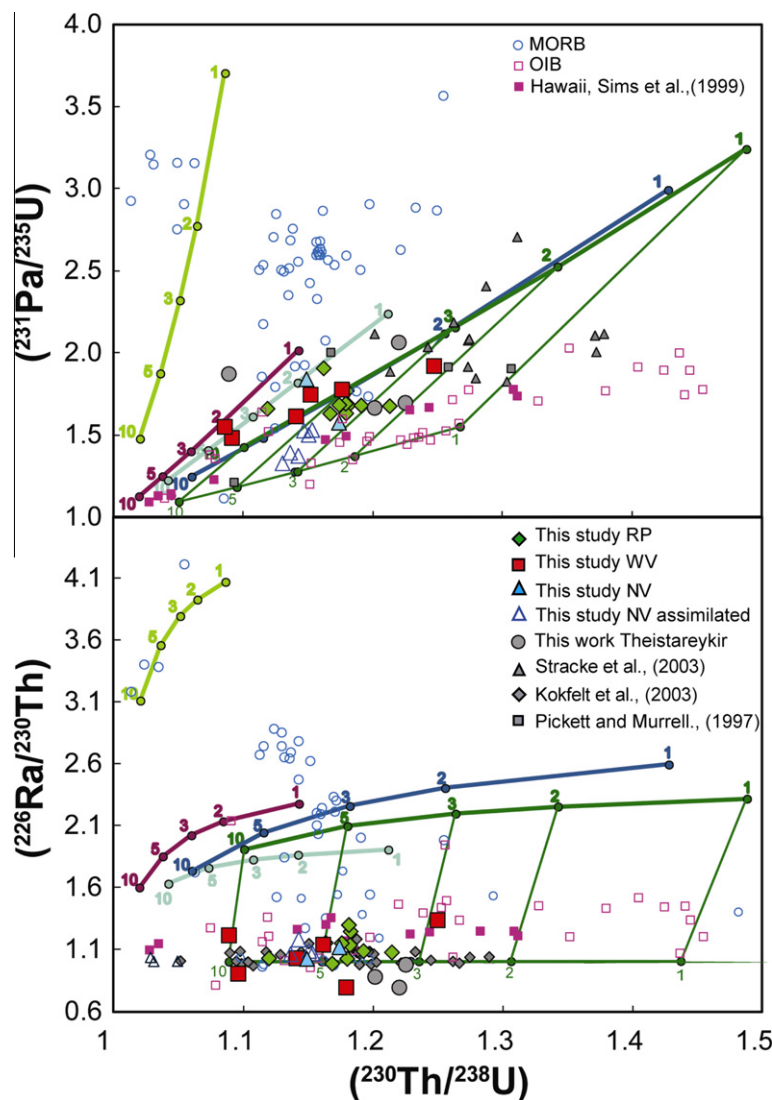
Fig. 4. Diagram of $(^{230}Th/^{238}U)$ versus $(^{231}Pa/^{235}U)$ and $(^{226}Ra/^{230}Th)$ showing Iceland data and OIB and MORB literature data. Model curves for dynamic melting of pyroxenite and peridotite sources are also displayed. The calculated variations in ^{230}Th and ^{231}Pa excesses are a function of mantle upwelling velocity indicated by coloured numbers (cm/yr). The green curves represent calculations for a spinel peridotite (light grey-green) and garnet peridotite (dark green) and are calculated using K_D values given in Table 2, the steep bright green curve is for a spinel peridotite calculated using partition coefficients for olivine and orthopyroxene from McDade et al. (2003a,b) and clinopyroxene from Wood et al. (1999); the purple and blue curves are calculated for a pyroxenite with low (purple) and high D_U/D_{Th} (blue), respectively (Table 2). The effect of decay during melt transport is shown for the garnet peridotite (thin green curves) at various upwelling velocities and for a melt velocity of 1 m/yr (lower green curve). OIB data from; Bourdon et al. (1998, 2005), Pickett and Murrell (1997), Prytulak and Elliott (2009), and Sims et al. (1999); MORB data from: Bourdon et al. (2005), Goldstein et al. (1993), Lundstrom et al. (1998, 1999), Sims et al. (1995, 2002), and Sturm et al. (2000). (For interpretation of the references to colour in this figure legend, the reader is referred to the web version of this article.)

nic (WV) samples show the largest variability with $(^{230}Th/^{238}U)$ ranging from 1.089 to 1.247, covering the full range of values measured in this study. Samples from the Northern Volcanic Zone (NV), excluding Theistareykir, have $(^{230}Th/^{238}U)$ ratios between 1.130 and 1.174, whereas samples from the Reykjanes Peninsula (RP) have $(^{230}Th/^{238}U)$ between 1.118 and 1.213. In a U–Th isochron diagram (Fig. 2a) NV samples show a positive correlation almost parallel to the equiline, whereas the RP samples generally have higher $(^{230}Th/^{232}Th)$ and $(^{238}U/^{232}Th)$ ratios. WV samples show large variation in $(^{230}Th/^{232}Th)$ at a lim-

ited range of $(^{238}U/^{232}Th)$, perpendicular to the trend of the NV samples (Fig. 2a).

3.2. ^{231}Pa–^{235}U disequilibria

$(^{231}Pa/^{235}U)$ ratios for Iceland's main rift lavas range between 1.333 and 1.925 (Table 1, Fig. 3). In a $(^{230}Th/^{238}U)$ versus $(^{231}Pa/^{235}U)$ diagram (Fig. 3a), the data form a broad positive trend. Three NV samples (NV41, NV52, NV54), however, plot below the general correlation with low $(^{231}Pa/^{235}U) \approx 1.33$–1.39 for a given $(^{230}Th/^{238}U) \approx 1.14$.

Similar to the ^{230}Th excesses, the ^{231}Pa excesses of samples from the Western Volcanic Zone cover the entire range of measured data. The sample from Hallmundarhraun (WV31) has the highest (^{231}Pa/^{235}U) and (^{230}Th/^{238}U) ratios; two other WV samples (WV25 and WV21) have the lowest measured (^{230}Th/^{238}U) of 1.09 at (^{231}Pa/^{235}U) of 1.49–1.55. Our new (^{231}Pa/^{235}U) data fall in between the data for Hawaiian basalts (Pickett and Murrell, 1997; Sims et al., 1999) and data for MORB (Goldstein et al., 1993; Sims et al., 1995, 2002; Lundstrom et al., 1998, 1999; Sturm et al., 2000; Bourdon et al., 2005; Turner et al., 2011), which generally have higher ^{231}Pa excesses at similar ^{230}Th excesses compared to OIB (Fig. 4). (^{230}Th/^{238}U) ratios in Icelandic lavas are similar to those measured in samples from the Azores (Bourdon et al., 2005; Prytulak and Elliott, 2009), but the (^{231}Pa/^{235}U) ratios are generally higher in the Icelandic rocks. In contrast to other OIB and MORB data the (^{231}Pa/^{235}U) ratios for the Iceland main rift samples (this study, Pickett and Murrell, 1997; Stracke et al., 2003a, 2006) correlate positively with (^{230}Th/^{232}Th) activity ratios (Fig. 2b).

3.3. ^{226}Ra–^{230}Th disequilibria

(^{226}Ra/^{230}Th) ratios range between 0.801 and 1.218, but the majority of the samples (21 out of 28, Table 1) have ^{226}Ra excesses. In agreement with the ^{230}Th and ^{231}Pa disequilibria data, samples from the Western Volcanic Zone show the largest variation almost covering the full measured range. The presence of ^{226}Ra excesses confirms that the samples are less than 8000 years old (Table 1). Two of the WV samples as well as the Theistareykir samples have ^{226}Ra deficits and thus an age younger than 8000 years is not confirmed. ^{226}Ra-deficits were also reported for OIB samples from the Azores and for the Pitcairn seamounts and were ascribed to alteration, crystal fractionation or to melting in the presence of phlogopite (Widom et al., 1992; Bourdon and Van Orman, 2009). (^{226}Ra/^{230}Th) ratios do not correlate with (^{230}Th/^{238}U) (Fig. 3c) and (^{231}Pa/^{235}U) ratios, nor with indicators of plagioclase fractionation (e.g., Sr) and potential indicators for the presence of phlogopite in the source (e.g., Nb/La). In the Theistareykir samples, a correlation of (^{226}Ra/^{230}Th) with (^{234}U/^{238}U) suggests that seawater alteration is responsible for the ^{226}Ra-deficits (see Section 3.4). The two WV samples with (^{226}Ra/^{230}Th) < 1, however, have (^{234}U/^{238}U) = 1 and their ^{226}Ra-deficits remain enigmatic.

3.4. Comparison of Theistareykir data with previous U-series data

The four samples from Theistareykir previously analysed by Stracke et al. (2003a, 2006) have (^{234}U/^{238}U) greater than 1 (Table 1). Stracke et al. (2003a) suspected that the high (^{234}U/^{238}U) obtained for these samples resulted partly from an analytical problem. However, we confirm here that the (^{234}U/^{238}U) are out of equilibrium, suggesting these samples were affected by seawater–rock interaction. The (^{230}Th/^{238}U) ratios measured previously by Stracke et al. (2003a) are consistently lower than those reported here,

due to the lower U concentrations determined by Stracke et al. (2003a). Two of the samples from Theistareykir that we re-analysed have significantly lower (^{231}Pa/^{235}U) (i.e., 10% and 22%) compared to those determined by Stracke et al. (2006) whereas the third sample is identical within analytical uncertainty. The higher ^{231}Pa-excesses measured by Stracke et al. (2003a, 2006) can thus be attributed to the lower U concentrations, but also result from higher Pa concentrations compared to those measured here. Note that the U concentrations obtained for BCR-2 and W2a confirm the accuracy of the technique employed here (Koornneef et al., 2010). Repeat analysis of WV31, a depleted sample from Iceland with 90 ppb U (Table 1), reproduced within 0.8%, which is indicative for the reproducibility of the low concentration Theistareykir samples. The Pa concentration determination for this sample (58 fg/g) reproduced to within 2.1%.

Stracke et al. (2003a, 2006) determined the U and Pa concentrations on separate sample aliquots in different laboratories, a strategy that is prone to error magnification (see discussion in Koornneef et al., 2010), which is one factor responsible for the observed discrepancy. Furthermore, the depleted nature of the Theistareykir samples renders those samples susceptible to seawater alteration. Seawater–rock interaction is expected to result in cm-scale heterogeneity and/or redistribution of U and hence highly heterogeneous U concentrations and U-series compositions at the sample scale. The fact that the Theisterykir sample with the highest (^{234}U/^{238}U) has the lowest (^{226}Ra/^{230}Th) also suggests that seawater alteration may play a role for creating the ^{226}Ra deficits. All samples from Theistareykir with evidence for seawater–rock interaction, i.e., (^{234}U/^{238}U) ≠ 1, presented in this study and reported in Stracke et al. (2006), are excluded from the following discussion.

4. INTERPRETING THE U-SERIES DATA

4.1. U-series melting models

Several U-series melting models have been proposed (e.g., McKenzie, 1985; Iwamori, 1993; Spiegelman and Elliott, 1993; Lundstrom et al., 1999; Jull et al., 2002). The difference in residence time between the parent and daughter nuclides causes in-growth of the daughter nuclide when the parent nuclide is retained preferentially in the solid residue during partial melting. Since the Iceland lavas show evidence for compositional variation created within melt channels (Maclennan et al., 2007; Stracke et al., 2003b; Maclennan, 2008b; Stracke and Bourdon, 2009; Koornneef et al., 2012), a dynamic melting model where melts do not re-equilibrate with their surrounding matrix appears most appropriate for interpreting the U-series data in Icelandic rocks (Claude-Ivanaj et al., 1998; Kokfelt et al., 2003; Bourdon et al., 2005, 2006; Prytulak and Elliott, 2009; Stracke et al., 2003a, 2006; Stracke and Bourdon, 2009). Moreover, recent experiments show that melts form interconnected melt networks at small degrees of melting (Zhu et al., 2011), suggesting that channelized melt transport may already be established during the initial stages of partial melt-

ing. The dynamic melting model, developed by McKenzie (1985), assumes that melts produced in the upwelling mantle 'escape' the solid residue after a critical threshold porosity is reached, with no further chemical interaction between the solid and melt (channelled melt flow). U, Th, Pa and Ra are all highly incompatible elements, and thus the U-series disequilibria are mostly formed at the onset of melting and reflect the conditions at the bottom of the melting region (Bourdon and Sims, 2003; Elliott et al., 2003; Iwamori, 1993, 1994; Stracke et al., 2006)In-growth of daughter nuclides in the dynamic melting model depends directly on the melting rate, which is a function of melt productivity and mantle upwelling velocity (McKenzie, 1985; Spiegelman and Elliott, 1993):

$$\Gamma = \rho_s^2 g W \left(\frac{dF}{dP} \right) \qquad (1)$$

where Γ is the melting rate in kg/m^3/s, ρ_s is the density of the solid in kg/m^3, g is the gravitational acceleration in m/s^2, W is the mantle upwelling velocity in m/s and (dF/ dP) is the amount of melt formed per increment of pressure release or melt productivity in% melt/GPa.

The melting model applied here is an incremental solution to dynamic melting and is described in detail in Stracke et al. (2003a, 2006). U-series disequilibria in instantaneous melts are calculated in a one-dimensional melting column assuming that the source is mineralogically homogeneous and initially in U-series secular equilibrium (i.e., undisturbed for >350 ka). Mineral-melt partition coefficients, source mineralogy and melt productivity in the model are a function of pressure (Stracke et al., 2003a). In contrast to the analytical solution of McKenzie (1985), which assumes infinite melt extraction velocity, varying melt extraction velocity (v) is possible, thereby accounting for radioactive decay during melt transport.

4.2. U-series nuclide partitioning

U-series nuclides are highly incompatible (Blundy and Wood, 2003) during peridotite melting and are exhausted from the residual mantle after 2–5% of partial melting. Garnet plays a key role for the fractionation between the U-series nuclides during melting because U is more compatible in garnet compared to Th, Pa and Ra (Beattie, 1993b; LaTourrette et al., 1993; Hauri et al., 1994; Salters and Longhi, 1999). In clinopyroxene (cpx), the partition coefficients are dependent on pressure and composition. Low Ca, aluminous cpx, which are typically present in high-pressure assemblages have higher D_U/D_{Th} compared to low pressure high Ca cpx. At the onset of melting cpx therefore significantly fractionates U from Th and Pa, albeit less than garnet (LaTourrette and Burnett, 1992; Beattie, 1993a; Hauri et al., 1994; Wood et al., 1999; Salters et al., 2002). Olivine and orthopyroxene do not significantly fractionate U-series nuclides (Blundy and Wood, 2003). As a consequence, melting of garnet-bearing assemblages with high D_U/D_{Th} yields melts with large ^{230}Th excesses, whereas melting of spinel peridotite with $D_U/D_{Th} \sim 1$ produces melts with no, or only small ^{230}Th excesses. However, the

absolute D_U and D_{Th} can be relatively large in spinel peridotites owing to the high $D_{U, Th}$ values in high Ca cpx (Wood et al., 1999; Salters et al., 2002; McDade et al., 2003b) resulting in substantial ^{231}Pa and ^{226}Ra excesses for only small ^{230}Th excesses (Stracke et al., 2006).

Experimentally determined mineral-melt partition coefficients for garnet and cpx in pyroxenite or eclogite (Klemme et al., 2002; Pertermann and Hirschmann, 2002; Pertermann et al., 2004; Elkins et al., 2008) overlap with partition coefficients determined for peridotite (Wood and Blundy, 1997; Salters et al., 2002; McDade et al., 2003a). Calculated bulk D_U/D_{Th} for pyroxenite range from being smaller to being larger than those in garnet-peridotite (Pertermann et al., 2004; Stracke et al., 2006; Elkins et al., 2008; Prytulak and Elliott, 2009). The magnitude of the U–Th fractionation and the difference in bulk partitioning behaviour of pyroxenite compared to peridotite thus remains poorly constrained.

4.3. Melt productivity

Melt productivity (dF/dP) has an important control on the melting rate (Eq. (1)). Melt productivity depends on the residual mineralogy and the coexisting liquid (e.g., Asimow et al., 1997). Theoretical and experimental studies show that melt productivity of peridotite increases with decreasing pressure and increasing melt fraction until one mineral phase is exhausted (Asimow et al., 1997, 2001; Hirschmann et al., 1998, 1999a; Stolper and Asimow, 2007). For U-series disequilibria, the near-solidus melting behaviour is particularly relevant, and ranges from 1% to ~5%/ GPa for peridotite (Asimow et al., 1997, 2001; Hirschmann et al., 1999b).

In contrast, near-solidus melt productivity of pyroxenite is substantially higher, about 13%/GPa (Pertermann and Hirschmann, 2003). In addition, pyroxenite is expected to start melting at similar or higher pressures compared to peridotite owing to its similar or lower solidus temperatures (McKenzie and Bickle, 1988; Pertermann and Hirschmann, 2003; Kogiso et al., 2004). Pertermann and Hirschmann (2003) showed that the melt productivity of synthetic pyroxenite G2 in their experiment increased up to 70%/ GPa before the onset of peridotite melting, partly due to heating of the pyroxenite by the enclosing peridotite. These characteristics potentially result in disproportionate contribution of the pyroxenite component to the final erupted melt (Hirschmann and Stolper, 1996; Stracke et al., 1999; Phipps Morgan, 2001; Pertermann and Hirschmann, 2003).

5. DISCUSSION

5.1. The role of crustal processes

Secondary processes such as crystallisation of phases that fractionate the U-series isotopes, radioactive decay during magma storage, and assimilation of hydrothermally altered wall rocks or evolved lavas potentially disturb the melting-induced U-series disequilibria.

U, Th, Pa and Ra are all highly incompatible in olivine, clinopyroxene and plagioclase (Blundy and Wood, 2003;

Fabbrizio et al., 2009), which crystallise in the tholeiitic basalts analysed here (Koornneef et al., 2012). Thus their activity ratios are not significantly affected by crystal removal during fractional crystallisation.

The melting-induced ^{230}Th, ^{231}Pa and ^{226}Ra excesses decay during long-term magma storage. This effect is most pronounced for ^{226}Ra because of its short half life ($T_{1/2} \sim$ 1.6 kyr) compared to ^{231}Pa ($T_{1/2} \sim$ 32 kyr) and ^{230}Th ($T_{1/2} \sim$ 75 kyr). Although samples from the Northern Volcanic Zone define a trend on a (^{230}Th/^{238}U) versus (^{231}Pa/^{235}U) diagram that is consistent with radioactive decay over a few tens of kyr (Fig. 3a), their ^{226}Ra excesses (Table 1) show that magma transport and storage time is less than 8 kyr. The NV samples with the lowest ^{230}Th- and ^{231}Pa- excesses, however, have slightly higher SiO$_2$ contents and lower MgO (4.7–7.8) than the WV and RP samples, indicative of more extensive fractional crystallisation. Kokfelt et al. (2009) attributed the variations in U-series disequilibria in lavas from the off-rift Snaefellsjökull volcano to the combined effects of crystal fractionation and radioactive decay. Unlike the main-rift tholeiitic basalts analysed here, samples from Snaefellsjökull range in composition from alkali basalt to trachyte and display clear relations between magma differentiation (e.g., MgO contents) and the U-series disequilibria. Based on the absence of such relations for our main-rift lavas, including samples from the Northern Volcanic Zone, (Fig. 5) both crystal settling and radioactive decay during magma differentiation

do not significantly influence the observed U–Th–Pa–Ra activity ratios.

Assimilation of crustal rocks or mixing with crustal melts in secular equilibrium could also lower the primary U-series disequilibria (e.g., Reubi et al., 2011). The samples from the Northern Volcanic Zone define a trend sub-parallel to the equiline suggesting mixing between a source with low U/Th and a source with high U/Th (Fig 2). Similar relationships for Icelandic basalts have previously been ascribed to assimilation of rhyolitic or dacitic crustal rocks or melts produced during shallow-level magma evolution. This process is especially important at central volcanoes where bimodal volcanism is observed, as for example Krafla and Askja in the Northern Volcanic Zone (Sigmarsson et al., 1991, 1992; Kokfelt et al., 2003; Chekol et al., 2011; Kuritani et al., 2011; Pietruszka et al., 2009). For the more evolved NV samples from the vicinity of the large central volcanoes Krafla and Askja, the relationships observed between (^{230}Th/^{232}Th), (^{238}U/^{232}Th), (^{231}Pa/^{235}U), and ratios of highly incompatible elements trace elements (e.g., Th/La, see Fig. 3e) (could therefore result from assimilation of evolved crustal melts or rocks. In a (^{230}Th/^{238}U) versus (^{231}Pa/^{235}U) diagram (Fig. 3a), the NV samples form a steep positive trend directed towards (^{230}Th/^{238}U) $\sim$ 1.08 and (^{231}Pa/^{235}U) = 1, potentially reflecting the composition of the assimilated rock, which must then be between about 160 and 375 kyr to explain the ^{230}Th excess of 8% and (^{231}Pa/^{235}U) in secular equilibrium. The assimilated rock
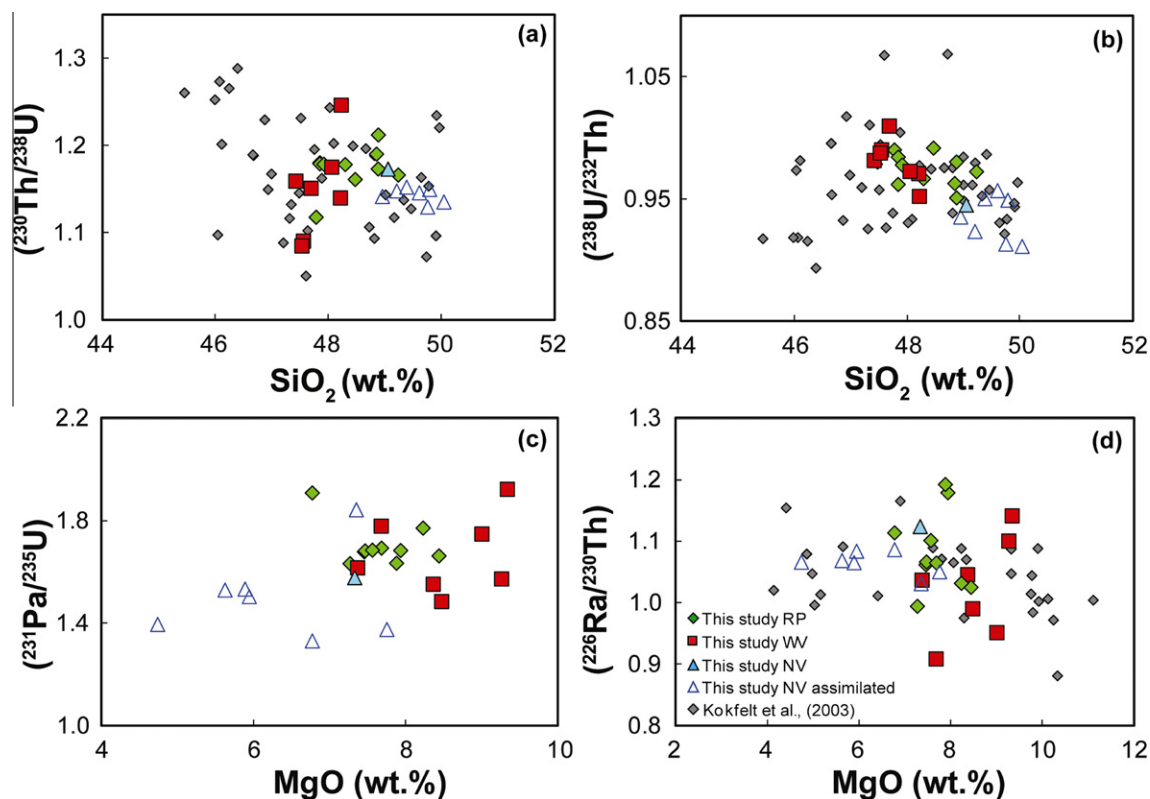

Fig. 5. U-series disequilibria data versus indices of magma differentiation (MgO and SiO$_2$). NV samples with the lowest ^{230}Th- and ^{231}Pa-excesses generally have slightly higher SiO$_2$ contents (open triangles Fig. 5a and b) and lower MgO (open triangles Fig. 5c and d). The lack of clear correlations suggests that magma storage is not a primary factor controlling the U-series disequilibria.

may thus represent a fractionated lava that stalled within the crust a few hundred ka ago.

A rhyolite from Askja volcano recently described by Kuritani et al. (2011) is used to test the bulk assimilation scenario discussed above. We approximate bulk assimilation by binary mixing between a depleted initial melt (e.g., NV49, Table 1) and a rhyolite that has Th = 7.16 ppm and U/Th = 0.28, (sample ID2405, Kuritani et al., 2011), $(^{226}Ra/^{230}Th)$ and $(^{231}Pa/^{235}U)$ in secular equilibrium and $(^{230}Th/^{238}U) = 1.08$. This mixing model reproduces the $(^{230}Th/^{232}Th)$, $(^{230}Th/^{238}U)$, $(^{231}Pa/^{235}U)$, $(^{226}Ra/^{230}Th)$ and $(^{238}U/^{232}Th)$ and the relationships between $(^{231}Pa/^{235}U)$ and Th/La, P_2O_5/Zr (Fig. 3e and f) of the NV samples and suggests about 7% of assimilation for samples NV52 and NV54 (see Fig. 3). Mixing with a rhyolitic rock or melt could also explain the slightly higher SiO_2 and incompatible trace element concentrations and the flatter HREE patterns observed in the NV samples that plot below the positive trend in a ^{231}Pa- versus ^{230}Th excess diagram (e.g., NV52, NV54, see Koornneef et al., 2012; Fig. 3a). Note that even though the combined lower $(^{226}Ra/^{230}Th)$ and $(^{231}Pa/^{235}U)$ ratios for the NV samples can be explained by bulk mixing with a rhyolite in $^{226}Ra-^{230}Th$ and $^{231}Pa-^{235}U$ equilibrium and a $(^{230}Th/^{238}U)$ of ∼1.08 (Fig. 3a and c), the ^{226}Ra excesses of the majority of the Icelandic samples are similarly low or lower than those of the NV samples at a large range of ^{231}Pa- and ^{230}Th excesses (Fig. 3c). This observation suggests that, for the remaining majority of the samples, other processes are responsible for the low ^{226}Ra excesses (Section 5.3).

We conclude that crustal processes do not influence the U-series systematics, with the potential exception of the more evolved samples from the Northern Volcanic Zone (all but NV49). These samples, which erupted close to large central volcanoes, show evidence for a possible effect of
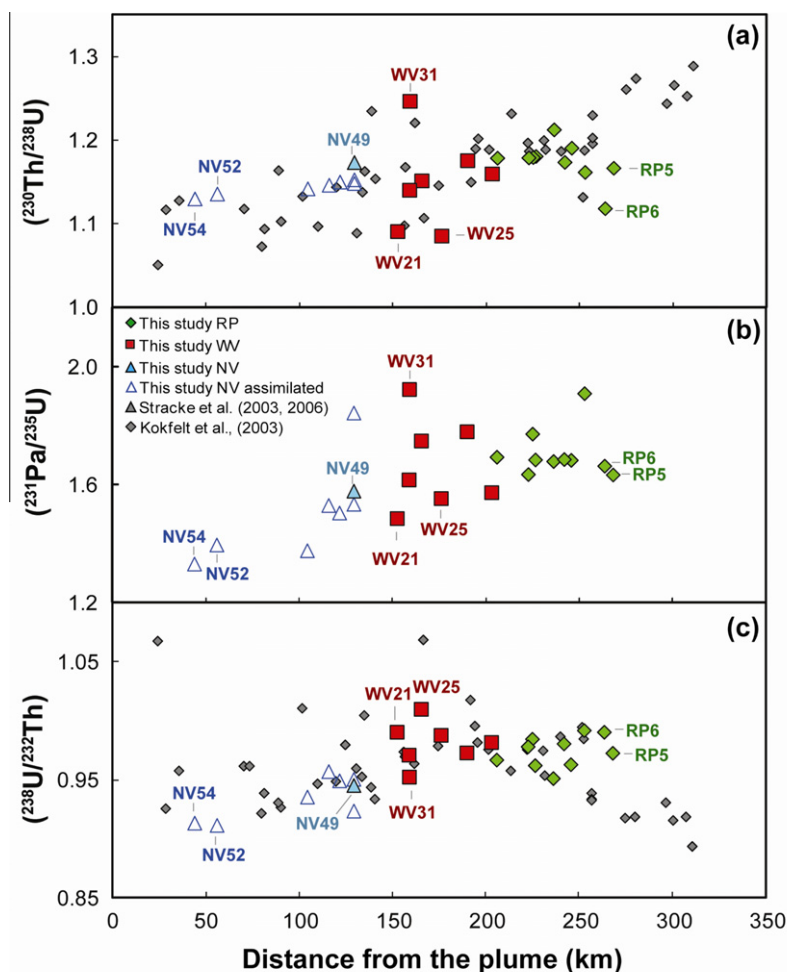

Fig. 6. U-series disequilibria for Iceland versus distance from the inferred plume centre. The $(^{230}Th/^{238}U)$ data for Iceland correlate with distance from the plume supporting a model of systematic increasing upwelling velocity towards the plume centre. This model is, however, not substantiated by the fewer existing $(^{231}Pa/^{235}U)$ data, which do not significantly correlate with distance from the plume centre. Furthermore, WV samples show considerable variability in $(^{230}Th/^{238}U)$ and $(^{231}Pa/^{235}U)$ even though these samples are collected from relatively small areas at similar distances from the plume centre. Note that NV samples that have relatively low ^{230}Th excess and the lowest ^{231}Pa excesses also have lower $(^{238}U/^{232}Th)$ activity ratios indicating the effect of assimilation. See text for further discussion. Samples specifically discussed in the text are labelled. Symbols are as in Fig. 5.

Table 2
Model input parameters.

		Depleted mantle				50–50 E-MORB crust
U (ppm)		0.0029				0.0452
Th (ppm		0.0092				0.135
Depth of melt initiation (km)		90				100
Residual porosity (%)		0.1				0.1
Productivity (%/km)	Onset	0.2			>90 km	0.5–2.3
	Final	2			<90 km	0.55
Final degree of melting (%)		20				40
Upwelling rate (cm/yr)		5				5
Melt extraction velocity		Infinitive				Infinitive
Peridotite						
Mineral mode		ol	opx	cpx	gt	sp
Gt field		0.53	0.08	0.34	0.05	0
Sp field		0.53	0.26	0.18	0	0.03
Partition coefficients (K_D)						
	ol	opx	hi Ca cpx	lo Ca cpx	gt	sp
U	0.00038	0.002	0.0113	0.0094	0.028	0
Th	0.00005	0.002	0.0057	0.0059	0.009	0
Bulk K_D						
		D_U	D_{Th}		D_U/D_{Th}	
Gt field		0.005603	0.002575		2.1765	
Sp field		0.002413	0.001609		1.500404	

	Pyroxenite 1		Pyroxenite 2	
Pyroxenite	Pertermann et al. (2004)		Pertermann et al. (2004)	
	Run A343		'Preferred'	
Mineral mode	cpx	gt	cpx	gt
	75	25	75	25
Partition coefficients (K_D)				
	cpx	gt	cpx	gt
D_U	0.0041	0.0045	0.0041	0.02405
D_{Th}	0.0032	0.0008	0.0032	0.00415
Bulk K_D				
	D_U	D_{Th}	D_U	D_{Th}
	0.42	0.26	0.90875	0.34375
		D_U/D_{Th}		D_U/D_{Th}
		1.615385		2.643636

mixing with crustal rhyolite based on their combined low ^{226}Ra, ^{231}Pa- and ^{230}Th excesses and low (^{238}U/^{232}Th) and will thus be excluded from further discussion of the U-series disequilibria in the context of partial melting.

5.2. Mantle upwelling velocity

5.2.1. Regional variability in the mantle upwelling

Dynamic melting of a homogeneous garnet-bearing peridotite source at variable upwelling velocities predicts positive correlations in diagrams of (^{230}Th/^{238}U) versus (^{231}Pa/^{235}U) (Fig. 6). Slow upwelling, corresponding to low melting rates, yields high ^{230}Th and ^{231}Pa excesses. Fast upwelling, corresponding to high melting rates, yields low ^{230}Th and ^{231}Pa-excesses. Using various sets of partition coefficients, modal mineralogy, depth of melt initiation, or melt extraction rate results in different trends with a positive slope (Fig. 6), with the exception for melting in the spinel stability field (applying the K_D values determined by McDade et al. (2003a), see also Stracke et al. (2006)).

Beneath Iceland's rift zones both active and passive mantle upwelling influence the mantle flow regime (Olson et al., 1993; Ribe et al., 1995; Ito et al., 1996; Maclennan et al., 2001; Shorttle et al., 2011). High mantle temperatures near the plume axis result in fast buoyancy-driven mantle upwelling, whereas further away, at lower mantle temperature, the upwelling is slower. This temperature-driven mantle flow regime is superimposed on the spreading ridge mantle flow regime, which is controlled by rifting of the lithosphere and passive mantle upwelling. At the ridge axis the mantle upwelling is primarily vertical and thus fast, but with increasing distance from the ridge the horizontal flow component becomes larger resulting in slower mantle upwelling (Ito et al., 1996; Ribe et al., 1995). Melts sampled from the regime farthest away from the spreading centre and the plume are thus expected to record slow melting rates and high ^{231}Pa and ^{230}Th excesses. Melts extracted from the on-axis regime close to the plume centre, on the other hand, should record faster melting rates and low ^{231}Pa and ^{230}Th excesses.
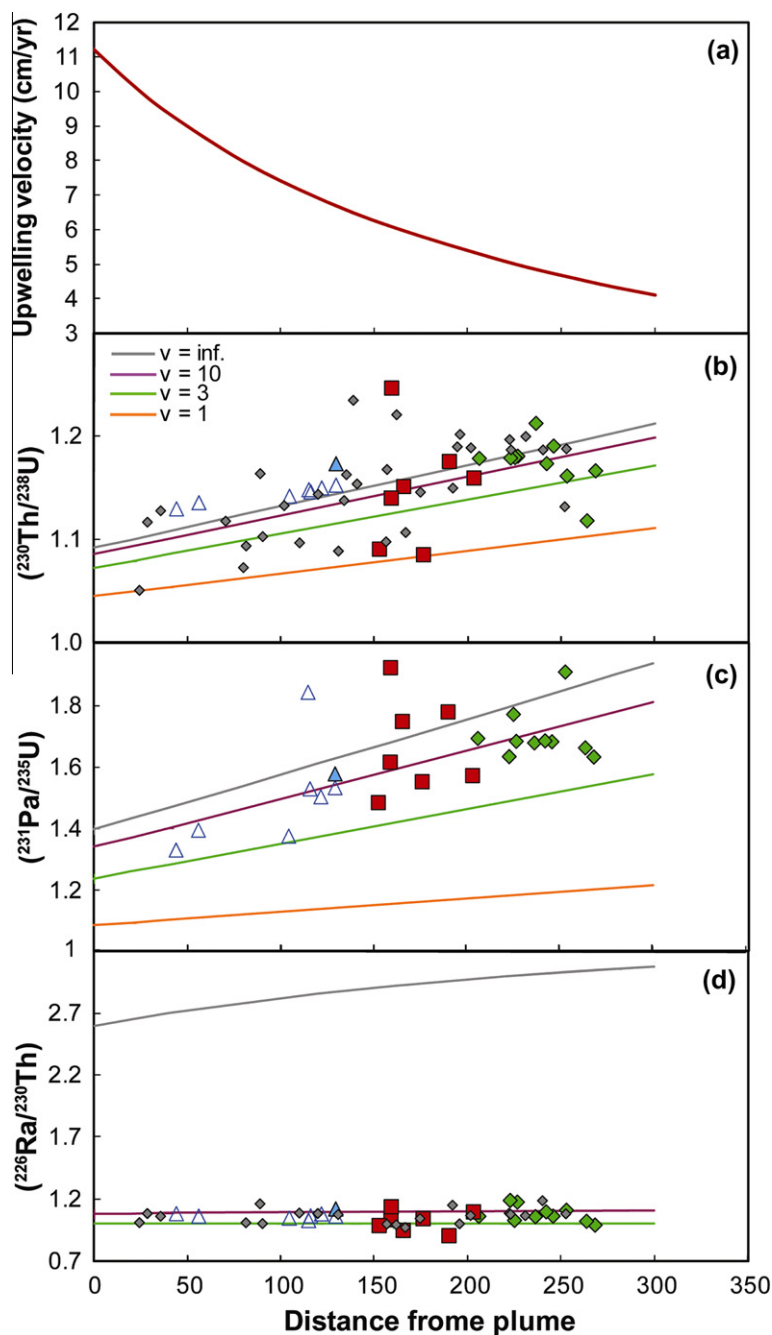
Fig. 7. (a and b) Estimated upwelling velocity with distance from the Iceland plume centre using dynamic melting of peridotite and the linear regression through (^{230}Th/^{238}U) in Icelandic main rift basalts measured by Kokfelt et al. (2003) and this study. The estimated mantle upwelling velocity across the Iceland plume ranges from 11.2 cm/yr at the plume axis to 4.1 cm/yr 300 km away from the plume. These estimates assume infinite melt extraction velocity. The effect of decay during melt transport is shown for melt velocities of $v = 10$, 3 and 1 m/yr. In this model the threshold porosity is set to 0.1%. (c and d) (^{231}Pa/^{235}U) and (^{226}Ra/^{230}Th) model predictions with distance from the plume for different melt velocities using the mean regression through (^{230}Th/^{238}U) as a reference. The relatively low ^{226}Ra excesses suggest that samples had melt velocities in between 3 and ~50 m/yr.

Kokfelt et al. (2003) suggested that a systematic increase in ^{230}Th excesses with distance from the plume centre in Iceland's rift zone lavas primarily reflects the radial, buoyancy–controlled, variation in the mantle upwelling velocity from 1–4 cm/yr at the margins of Iceland to 5–20 cm/yr in the centre of the plume (Kokfelt et al., 2003).

In Fig. 6, (^{230}Th/^{238}U), (^{231}Pa/^{235}U) and (^{238}U/^{232}Th) ratios are plotted against distance from the inferred plume centre, showing that the ^{230}Th excesses increase with distance from the plume centre. The variability in ^{230}Th-excesses (Fig. 5a) is consistent with the data of Kokfelt et al. (2003), although there is slightly larger variability

on a local scale, most conspicuous for the samples from the Western Volcanic Zone (Fig. 6a). A Spearman Rank test for the (^{230}Th/^{238}U) data, including the Kokfelt et al. (2003) main rift data but excluding the evolved NV samples, yields a correlation coefficient (rho) of 0.55 ($n = 49$), indicating a significant correlation (confidence level >95%). The correlation thus supports the model of increasing mantle upwelling velocities towards the plume centre. The estimated range in upwelling velocities assuming dynamic melting of a homogeneous peridotite source (Table 2) is in agreement with the estimates of Kokfelt et al. (2003) (Fig. 7a). In this estimation, the mean (^{230}Th/^{238}U) ratios as a function of distance from the plume centre (see Fig. 7a) are used to estimate the mantle upwelling velocity (W) across the Icelandic thermal anomaly. Extrapolation of the regression line to the centre of the plume yields a (^{230}Th/^{238}U) of 1.092, which, in the dynamic melting model corresponds to a mantle upwelling velocity of 11.3 cm/yr. The mean (^{230}Th/^{238}U) 300 km away from the plume centre is 1.212, corresponding to a mantle upwelling velocity of 4.1 cm/yr. Note that these estimates are only indicative given the relatively broad nature of the relationship between the ^{230}Th excesses and distance from the plume. Furthermore, the estimates are highly dependent on the model parameters used, such as the partition coefficients and melt productivity function. For example, using an initial melt productivity of 0.3%/km rather than 0.2%/km would correspond to a W of 8 cm/yr at the centre of the plume and a W of 3 cm/yr at a distance of 300 km.

The ^{231}Pa excesses are expected to show a more pronounced relationship with distance from the plume than the ^{230}Th excesses owing to the shorter half-life of ^{231}Pa compared to ^{230}Th (~32 ka versus ~75 ka, respectively). However, the (^{231}Pa/^{235}U) data, excluding the NV samples close to the plume centre that show evidence for assimilation, do not correlate significantly with distance from the plume given the Spearman's rank correlation coefficient of 0.24 ($n = 18$). The lack of correlation likely results from the limited number of data, but could also reflect the influence of melt velocity, porosity and/or source heterogeneity (see Sections 5.3 and 5.4), which have a comparatively greater effect on the (^{231}Pa/^{235}U) than on the (^{230}Th/^{238}U) ratios.

In the (^{230}Th/^{238}U) versus (^{231}Pa/^{235}U) diagram (Fig. 4a), the Icelandic main rift data define a broad positive array. Compared to the Hawaiian samples (Sims et al., 1999), the Icelandic data are, however, much more variable. Samples collected from closely spaced eruptive centres in the Western Volcanic Zone, for example, have highly variable (^{230}Th/^{238}U) and (^{231}Pa/^{235}U) ratios, comparable to the regional range in disequilibria data (Figs. 5a, b and 6). The observed local variability and the lack of a correlation of the (^{231}Pa/^{235}U) data with distance from the plume suggest that the ^{231}Pa-excesses are not primarily controlled by regional mantle upwelling velocity.

5.2.2. Local variability in upwelling velocity

One reason for the observed local range in ^{230}Th and ^{231}Pa excesses could be variable melting rates during partial melting, due to variations in mantle upwelling velocities within the local melting region.

Glacial unloading during early post-glacial times, at about 10,000 years ago is a possible cause of variable mantle upwelling velocity on a local scale (Jull and McKenzie, 1996; Gee et al., 1998; Maclennan et al., 2002). However, most samples investigated in this study are all younger than 5300 yr, and should thus not be affected by temporally variable upwelling velocity due to glacial unloading.

Changing mantle viscosity due to dehydration melting (Ito et al., 1999; Maclennan et al., 2001; Kokfelt et al., 2003) could also produce 'vertical' variation in upwelling velocity within a given melting region. As a result, local variability in ^{230}Th and ^{231}Pa excesses in erupted lavas integrating over variable depth ranges of the melting region would be expected. Large variability in trace element ratios that are sensitive to the degree of melting, e.g., La/Sm and La/Yb, in Icelandic lavas indicate that melts are indeed extracted from, and integrate over, different depths of the melting region (Wood, 1981; Elliott et al., 1991; Maclennan et al., 2003, 2007; Stracke et al., 2003b; Kokfelt et al., 2006; Koornneef et al., 2012). The lack of correlation between La/Sm and (^{230}Th/^{238}U) or (^{231}Pa/^{235}U), however, confirms that the U-series disequilibria, due to the incompatibility of the U-series nuclides, are little influenced by progressive melting, and are primarily established during the initial stages of melting. Hence, vertical variation in upwelling velocity is unlikely to be resolved by the U-series and thus cannot explain the local variability in U-series disequilibria.

Mantle upwelling velocity also varies laterally within the local sub-ridge melting region. As discussed above, mantle flow is primarily vertical and thus fast at the ridge axis, but becomes slower with increasing distance from the ridge axis due to increasingly horizontal mantle flow (Ito et al., 1996; Ribe et al., 1995). Melts generated farthest away from the spreading centre are thus produced with slower melting rates and are expected to have higher ^{231}Pa and ^{230}Th excesses than those generated on-axis. To explain the largest and smallest ^{230}Th excesses within the WV group (i.e., 24.7% for WV31 and 8.5% for WV25) by lateral variations in mantle upwelling velocities within the local melting region, requires variation in local mantle upwelling velocity from about 2 to 10 cm/yr, assuming melting of a garnet peridotite source (Fig. 4, Table 2). Sample WV31 could in this scenario results from melting slowly upwelling mantle furthest away from the spreading ridge, whereas sample WV25 could results from melting faster upwelling mantle closer to the spreading ridge. Note that this model requires that the melts formed at different parts in the 3-D melt region migrate over various distances to erupt at the rift axis (see Section 5.3.1).

In addition to variable local mantle upwelling velocity, differences in melt extraction velocity, mantle porosity, or source lithology could be important for establishing the observed local-scale variability in U-series disequilibria, and will be discussed in the following.

5.3. Melt transport velocity and mantle porosity

5.3.1. Melt transport velocity

Rather than from variable upwelling velocity, the local variations in U-series disequilibria could result from varia-

tions in melt transport velocity and/or mantle porosity on a local scale. In order to estimate the upwelling velocity beneath Iceland in Section 5.2.1 (Fig. 7) it was assumed that
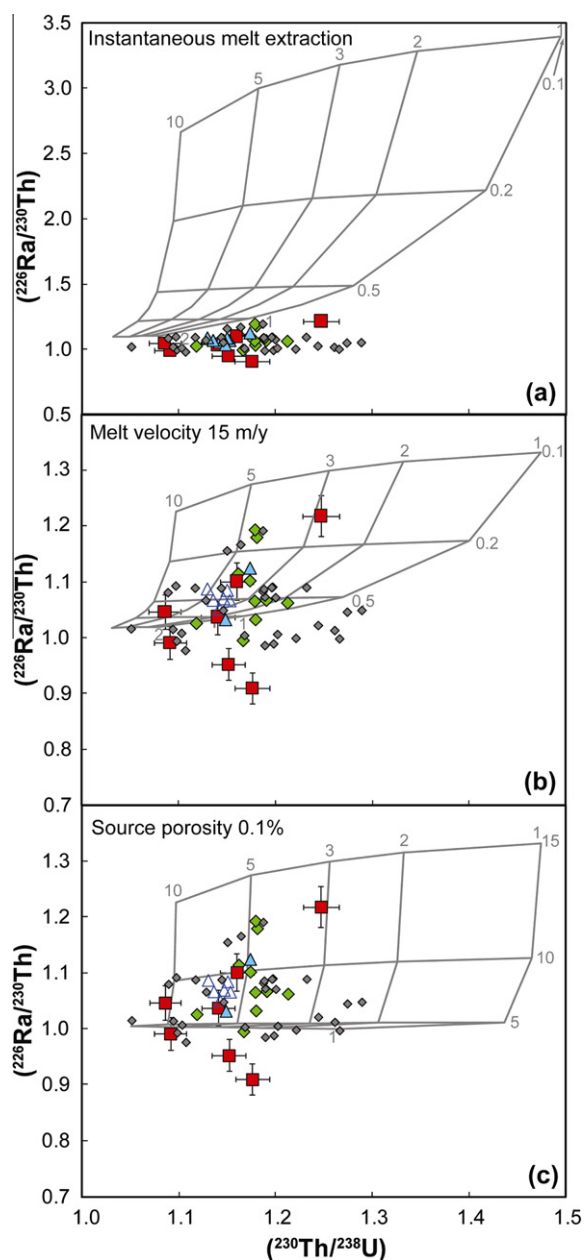

Fig. 8. Dynamic melting model for variable upwelling velocities using different mantle porosities but assuming instantaneous melt extraction (a), melt extraction of 15 m/yr (b), or using a constant source porosity but variable melt extraction velocities (c). Horizontal curves represent predicted disequilibria for variable upwelling velocities at a fixed porosity or melt extraction velocity, whereas vertical, kinked curves are calculated for variable p or v at a fixed upwelling velocity. The combined ^{226}Ra–^{230}Th excesses measured for Iceland can be explained by porosities ranging between 0.1% and 2% at a melt transport time of 15 m/yr. Note, however, that the variability could also be explained by variations in melt velocities at a given threshold porosity.

the samples were not significantly affected by decay during melt transport (i.e., melt transport time is short relative to the half life of the daughter nuclides). However, the relatively low measured ^{231}Pa and ^{226}Ra excesses compared to the predicted mean trend for infinite melt extraction velocity (Figs. 4b, 7c and d), suggest that melt velocity is not infinite, but varies between 3 and 50 m/yr. Thus, decay during melt transport influences the U-series disequilibria of the Icelandic melts considerably (e.g., Stracke et al., 2003a). Extraction of melts from different parts in the 3-D mantle flow regime underneath the Icelandic rift zone, as discussed in Section 5.2, is expected to give rise to variability in melt transport times. Melt transport with a significant horizontal component is thought to be 1–2 orders of magnitude slower compared to buoyancy-driven vertical melt transport (Braun and Sohn, 2003; Ruedas et al., 2004). The time it takes for melts to reach the axis depends on their initial lateral distance from the ridge axis (Katz, 2008). Melts formed in the mantle flow regime far from the ridge axis require migration over both a longer distance and with a larger horizontal component compared to melts that are derived from the mantle directly underneath the ridge. Hence these melts may experience relatively more radioactive decay of the primary melting induced U-series excesses compared to melts formed directly below the ridge axis, which is especially important for the ^{226}Ra-excesses. Lavas derived from the mantle far away from the ridge are thus expected to have initially high ^{230}Th, ^{231}Pa and ^{226}Ra excesses from melting at slow mantle upwelling velocity. However, especially their ^{226}Ra excesses decay considerably during transport towards the rift. Sample WV31, the sample with the largest ^{230}Th and ^{231}Pa- excesses in the Western Volcanic Zone, which could thus have such an off-axis origin has (^{226}Ra/^{230}Th) = 1.218. The two WV samples with the lowest ^{230}Th, ^{231}Pa- excesses WV21 and WV25, which suggest fast mantle melting rates and thus generation closer to the ridge axis, however, have no ^{226}Ra excesses (Table 1). The higher Ra-excesses for WV31 compared to WV21 and WV25 are hence inconsistent with the scenario that WV31 melts travelled over a longer distance and originate from melting farther from the ridge compared to the WV21 and WV25 melts. Thus, the hypothesis that variability in the (^{230}Th/^{238}U) or (^{231}Pa/^{235}U) for the Western Volcanic Zone result from variations in local mantle upwelling velocity in the sub-ridge melt region as discussed in Section 5.2.2, is not supported by expected variations in (^{226}Ra/^{230}Th) considering differences in melt transport time.

5.3.2. Residual porosity

The threshold porosity of the mantle is another important parameter in the dynamic melting model as it defines the melt fraction in equilibrium with the residue before the melt is extracted. The larger the porosity, the less is the fractionation between parent and daughter nuclides, and thus less daughter nuclides are produced in the residual mantle during melting. The threshold porosity is especially important for the ^{226}Ra with its shorter half-life compared to ^{230}Th and ^{231}Pa.

The observed ^{226}Ra-excesses in OIB, generally suggest partial melting at low porosities (<<1%), although literature estimates range over an order of magnitude (Spiegelman and Elliott, 1993; Sims et al., 1999; Slater et al., 2001; Elliott et al., 2003). The calculations shown in Figs. 4 and 7 assume melting at a constant porosity of 0.1%. Model curves for varying porosity and upwelling velocity at infinite melt extraction velocity are plotted in Fig. 8a. The model predicts relatively low ^{226}Ra- excesses with a narrow range in ^{230}Th excesses for large threshold porosities (up to 2%) and relatively high ^{226}Ra- excesses with a large range in ^{230}Th excesses for small threshold porosities (0.1%, Fig. 8a). The predicted ^{226}Ra excesses for a given ^{230}Th excess in the model are larger than those observed for Icelandic samples even for the largest porosities. Hence the significant range of ^{230}Th at low ^{226}Ra excesses observed in the Icelandic rift lavas is incompatible with large residual porosity and infinite melt extraction velocity (Fig. 8a). This observation confirms that decay during melt transport must have an important effect on the ^{226}Ra-^{2}disequilibria (Fig. 7, Stracke et al., 2003a). The variability in ^{226}Ra disequilibria for Iceland shown in Fig. 8 can be explained by mantle porosities between 0.1% and 2%, with melt transport velocities of about 15 m/yr (Fig. 8b). Note, however, that the variability can similarly be explained by variations in melt velocities at a given threshold porosity (Fig. 8c). Thus it is difficult to distinguish between the relative effects of these two parameters, but they are likely the controlling parameters for the observed variability in ^{226}Ra-excesses, both on a local, and regional scale. The ^{226}Ra-deficits determined for the two WV samples can, however, not be explained by variations in melt velocity or porosity and remain enigmatic.

5.4. The influence of source heterogeneity

Variability in mantle upwelling velocity and variable transport times both influence the Icelandic rift zone lavas, but appear not to be the primary controlling processes in generating the large variation in ^{230}Th and ^{231}Pa-excesses for WV samples collected from closely spaced eruptive centres. The role of residual mantle porosity is ambiguous, but is negligible for creating the variable (^{230}Th/^{238}U) and (^{231}Pa/^{235}U) ratios. In the following, we thus evaluate the effect of source heterogeneity on the U-series disequilibria of the WV samples.

Melting rates can vary significantly between sources of different mineralogical composition that have different melt productivity. Pyroxenite, for example, has a larger melt productivity than peridotite, resulting in a higher melting rate (e.g., Hirschmann and Stolper, 1996; Stracke et al., 1999; Pertermann and Hirschmann, 2003; Prytulak and Elliott, 2009) (Section 4.3). The presence of small-scale source heterogeneity, inferred to represent pyroxenitic recycled oceanic crust (Chauvel and Hémond, 2000; Hanan et al., 2000; Skovgaard et al., 2001; Stracke et al., 2003b; Kokfelt et al., 2006; Stracke and Bourdon, 2009) could therefore significantly affect the U-series disequilibria in Icelandic basalts.

Strong depletion in Rb, Ba, U and Th and enrichment in Nb and Ta compared to La observed in the most enriched

Icelandic samples suggest that the recycled component represents ancient E-MORB crust (McKenzie et al., 2004; Koornneef et al., 2012). Variable enrichments indicated by high Nb/La and Nb/U and radiogenic Pb isotopes for main rift lavas further suggest that the proportion of the mafic recycled component is variable beneath the different main rift areas or that the component is intrinsically heterogeneous in highly incompatible element composition (Koornneef et al., 2012). In the Northern Volcanic Zone, including Theistareykir, enrichments in highly incompatible trace elements are relatively limited indicating that the abundance of the mafic component is small. In contrast, beneath the Western Volcanic Zone and the Reykjanes Peninsula, larger and highly variable enrichments in highly incompatible trace elements suggest that the enriched component is more abundant but also heterogeneously distributed. Therefore, the hypothesis to be tested in the following
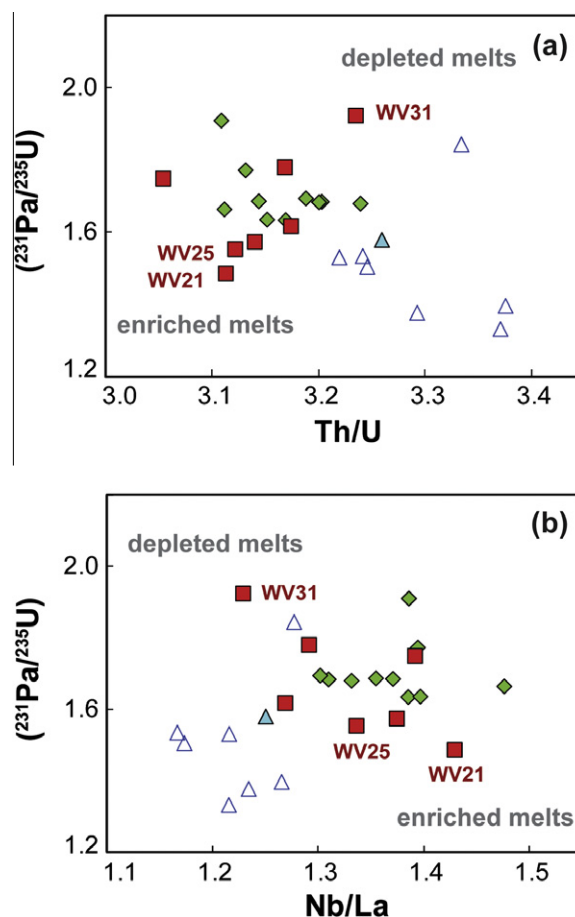

Fig. 9. Plots of (^{231}Pa/^{235}U) versus highly incompatible trace element ratios. Samples from the Western Volcanic Zone show relations that suggest the influence of source heterogeneity. The relations suggest that samples with low ^{231}Pa excesses and Th/U but high Nb/La (WV21, W25) were produced with a higher melting rate than more depleted ones (high ^{231}Pa excesses but low Nb/La, WV31). The combined U-series and highly incompatible trace element characteristics of WV samples thus argue for the influence of a mafic component with low Th/U but high Nb/La and high melt productivity.

is that samples with the highest $(^{230}Th/^{238}U)$ ratios on a local scale represent melts with a dominant peridotite melt signature that reflects low melt productivity, whereas samples with the lowest $(^{230}Th/^{238}U)$ represent aggregated melts with a higher contribution of melts from the enriched source component, which have been generated with higher melt productivity.

5.4.1. Evidence for variable melting behaviour?

Two samples from the Western Volcanic Zone (WV21 and WV 25) have relatively low ^{230}Th-excesses compared to other samples but moderate ^{231}Pa-excess. Sample WV25 for example, has $(^{230}Th/^{238}U)$ of 1.09 and $(^{231}Pa/^{235}U)$ ratio of 1.55. This observation requires that the source for these samples has relatively low bulk D_U/D_{Th} at moderately high bulk D_U to account for the small ^{230}Th excesses and moderately high ^{231}Pa excesses. One potential explanation for this apparent bulk partitioning behaviour would be shallow melting in the spinel peridotite stability field (Fig 6). However, relatively high Sm/Yb (WV25 has Sm/Yb$_N$ = 1.66, Fig. 10a), Lu/Hf, and Tb/Yb for these two WV samples suggest a greater, not smaller, contribution of melts from the garnet-field compared to other WV samples. Rather than resulting from melting in the spinel stability field, the low ^{230}Th excesses and high Sm/Yb of sample WV21 and WV25 thus argue for melting a garnet-rich lithology with low D_U/D_{Th} (Fig. 4). Low bulk D_U/D_{Th} ($\sim$1.6) was determined experimentally for pyroxenite by Pertermann et al. (2004, their experiment A343). Furthermore, the low ^{230}Th and ^{231}Pa excesses in the two WV samples and broad correlations with Th/U and Nb/La ratios (Fig. 9) suggest that more enriched samples (WV21, W25) were produced with a higher melting rate (low ^{230}Th and ^{231}Pa excesses) than more depleted ones (high ^{230}Th and ^{231}Pa excesses, WV31). Hence the combined U-series and trace element characteristics of WV samples argue for the influence of a mafic component with low D_U/D_{Th} and high melt productivity.

5.4.2. The relation between $(^{230}Th/^{232}Th)$ and ^{231}Pa excesses

An intriguing observation for the Icelandic data is that there is a good correlation between ^{231}Pa excesses and $(^{230}Th/^{232}Th)$ activity ratios for samples from all rift zones. Kokfelt et al. (2009) found a similar correlation for lavas from the off-rift Snaefellsjökull volcano and ascribed the correlation to crystal fractionation and decay of the lavas at this large central volcano. Note, however, that the observed relation for main rift samples cannot be explained by fractionation and radioactive decay (except for the more evolved NV samples, Section 5.1, Fig. 3d) and thus requires another explanation. Compared with other OIB localities, Iceland is the only ocean island that displays such a trend (Fig. 2b) indicating that the processes responsible for this correlation are unique to Iceland, rather than being a general feature of upper mantle melting.

The $(^{231}Pa/^{235}U)$ and $(^{230}Th/^{232}Th)$ activity ratios are a function of the time available for ingrowth or decay of the daughter products and the partition coefficients of U and the D_U/D_{Th}. However, only the $(^{230}Th/^{232}Th)$ ratio is in addition controlled by the U/Th ratio of the source,

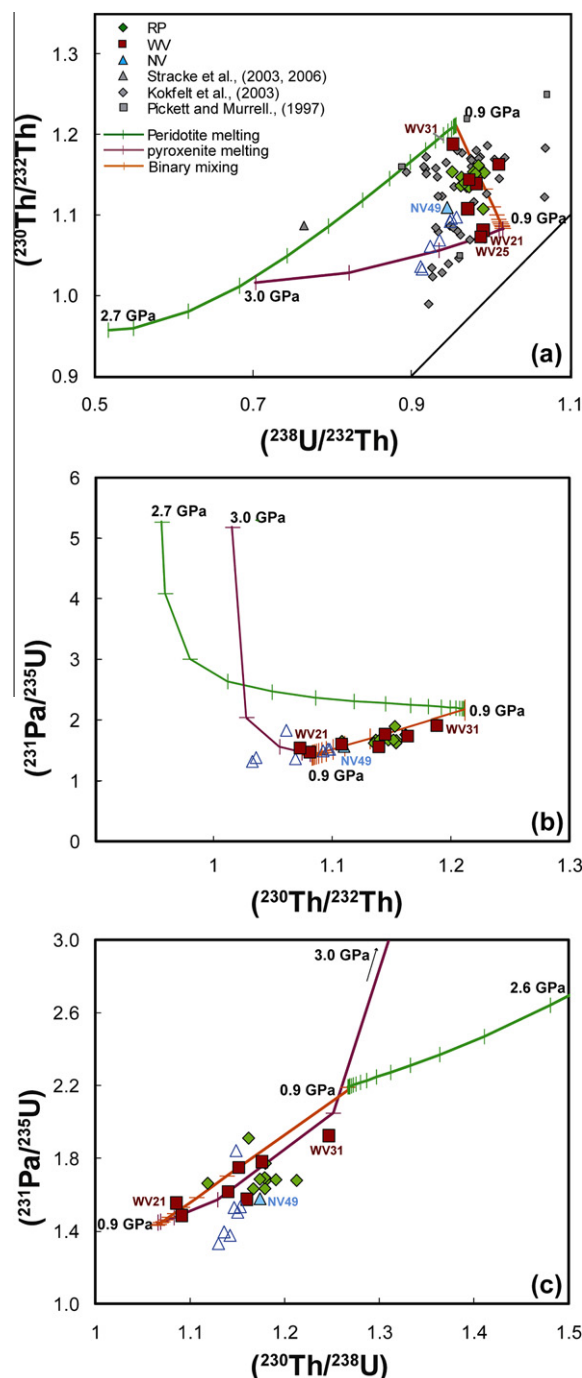Fig. 10. Diagrams of (a) $(^{230}Th/^{238}U)$ versus $(^{231}Pa/^{235}U)$, (b) $(^{230}Th/^{232}Th)$ versus $(^{231}Pa/^{235}U)$ and (c) $(^{226}Ra/^{230}Th)$ versus $(^{231}Pa/^{235}U)$ showing melting curves for a garnet peridotite (green) and a pyroxenite (purple) with low D_U/D_{Th} that has high melt productivity (Table 2). Tick marks on the melting curves represent compositions at 0.03 GPa pressure intervals ($\sim$1 km depth intervals). Upwelling velocity is assumed to be constant and (5 cm/yr), which is the estimated upwelling velocity at $\sim$150 km distance from the plume, where the WV samples erupted (see Fig. 7). Binary mixing between the final accumulated melts is shown in orange. Tick marks on binary mixing curves represent 10% increments. Samples specifically discussed in the text are labelled. (For interpretation of the references to colour in this figure legend, the reader is referred to the web version of this article.)
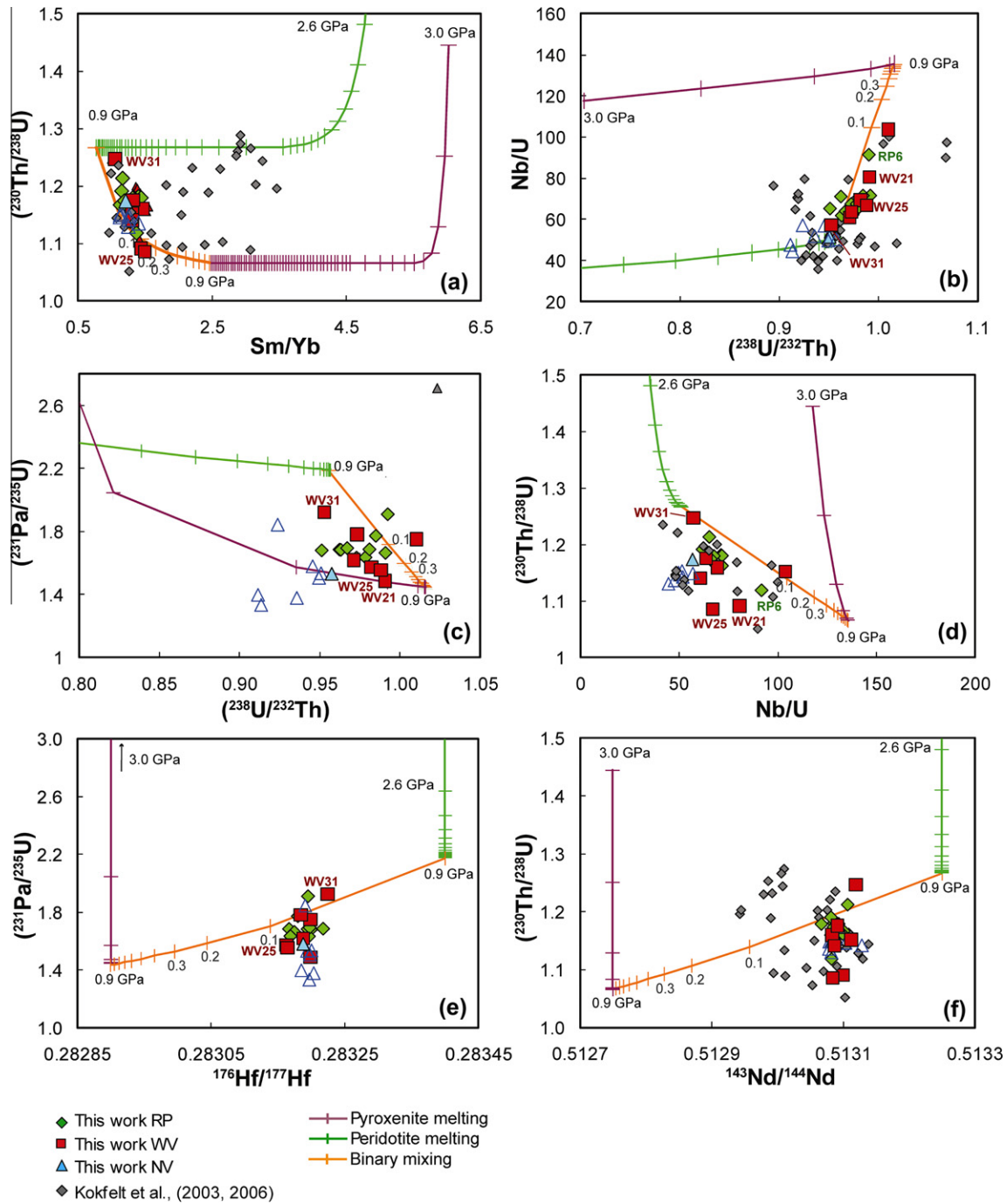
Fig. 11. Combined trace element and Hf and Nd isotope ratios against (^{230}Th/^{238}U) and (^{231}Pa/^{235}U) with melting curves for a garnet peridotite and a pyroxenite (Table 2) and binary mixing curves where tick marks represent 10% increments of mixing between the peridotite and pyroxenite melts. The upwelling velocity in these calculations is constant (5 cm/yr). Samples specifically discussed in the text are labelled in grey.

whereas the (^{231}Pa/^{235}U) is not. Higher initial U/Th source ratios are expected to result in higher (^{230}Th/^{232}Th) ratios in the derivative melts, but have no influence on the (^{231}Pa/^{235}U) ratios. Hence the correlation between (^{231}Pa/^{235}U) and (^{230}Th/^{232}Th) activity ratios provides information about the melting behaviour of the different source components.

It was suggested above that WV samples WV25 and WV21 with low (^{230}Th/^{238}U) but high U/Th result from melting an enriched source with low bulk D_U/D_{Th} at high melt productivity. These samples form the local enriched 'end-member' for the Western Volcanic sample suite, whereas the depleted WV31 sample, forms the local depleted 'end-member'. This sample has the highest ^{231}Pa

excesses and high (^{230}Th/^{232}Th), but has a moderate U/Th ratio, which requires melting of a source with high bulk D_U/D_{Th} (Fig. 10b). The high ^{230}Th and ^{231}Pa-excess recorded by this end-member can be explained by relatively low melt productivity for the depleted peridotite source in combination with relatively slow mantle upwelling at moderate distance from the plume axis.

Note that sample NV 49, i.e., the only NV sample that appears not to be affected by crustal processes, has a very different U/Th ratio compared to enriched WV samples, but that their (^{230}Th/^{232}Th) and (^{231}Pa/^{235}U) are both low (e.g., Fig. 10b). This NV sample with low (^{230}Th/^{238}U) and (^{231}Pa/^{235}U) could result from initial melting of a source with relatively low U/Th requiring different melting behaviour than the WV samples. If the WV lavas with low (^{230}Th/^{238}U) but high U/Th are formed by melting an enriched source at low bulk D_U/D_{Th} the NV samples with similarly low (^{230}Th/^{232}Th) and (^{231}Pa/^{235}U) as WV25 and WV21 but low U/Th could reflect initial melting of a depleted mantle source with a comparatively higher D_U/D_{Th}.

5.4.3. Relationships between U-series and Hf and Nd isotopes

Data for Iceland in diagrams of U-series disequilibria against Hf and Nd isotopes show ambiguous relationships. Although the highly depleted sample WV31, with higher ^{231}Pa and ^{230}Th-excesses in general have higher Nd isotope composition compared to the other samples (Fig. 11e and f), U-series data for RP and NV samples do not correlate with ^{143}Nd/^{144}Nd. A positive correlation between (^{231}Pa/^{235}U) and Hf isotopic composition is only observed on a local scale, i.e., for the WV samples, which supports melting and mixing of melts from two mantle source components beneath the Western Volcanic Zone (Fig 11e). The lack of a general correlation for Iceland between long-lived isotopes and U-series disequilibria suggests that the regional trends in ^{230}Th- and ^{231}Pa excesses with distance from the plume are not primarily controlled by source composition. Note, however, that due to extraction of melts from variable depths and incomplete melt mixing, relationships between U-series activity ratios and Hf–Nd isotope ratios are not necessarily expected (Koornneef et al., 2012). Where the degree of melting and mixing produces systematic variability in trace element ratios including a moderately incompatible element, e.g., La/Yb or Nd and Hf isotope ratios, during progressive melting, highly incompatible trace elements element ratios, e.g., Nb/U or (^{231}Pa/^{235}U), do not change after the first few percents of melting.

5.4.4. Mixing melts from a two-component source

Mixing between melts from a pyroxenite component and melts from the surrounding peridotite is a possible mechanism to create the large local-scale variability in ^{230}Th and ^{231}Pa excesses observed in the Western Volcanic Zone and the Reykjanes Peninsula. The hypothesis is tested using a mixing model combined with the dynamic melting model for two source components that have different modal mineralogy, partitioning characteristics, and melting behaviour (Table 2). The model applied here (Section 4.1, Table 2) calculates compositions of instantaneous melts from two sources (depleted mantle and pyroxenite 1 in Table 2) sep-

arately, and mixes the melts according to their final relative mass fractions. For simplicity we assume that the U-series disequilibria for samples erupting at a small range in distances from the plume centre (e.g., WV samples, 150–180 km, Fig. 5) result from melting at a constant mantle upwelling velocity of 5 cm/yr.

The Nb/U, Nb/La and La/U ratios in Iceland main rift lavas correlate well with U/Th ratios suggesting that the enriched component is characterised by high Nb/U, Nb/La and U/Th ratio, the depleted component has a low U/Th (Fig. 11b). Note that this is opposite to what is has been inferred for other spreading ridges (e.g., EPR, Goldstein et al., 1993; Lundstrom et al., 1999) where the U/Th ratio of depleted samples is typically higher compared to enriched samples. Even though the variability in U/Th for Iceland's main rift lavas is small (0.301–0.333) the correlation with tracers for enrichment (Fig. 10b) is conspicuous. WV Samples with higher U/Th and Nb/U but low Hf isotope ratios have lower (^{231}Pa/^{235}U) and (^{230}Th/^{238}U) (Fig. 11) whereas WV31, which has low U/Th and Nb/U and high Hf isotope ratios, has the highest ^{231}Pa and ^{230}Th excesses.

Koornneef et al. (2012) have discussed the importance of mixing of melts during melt extraction using a polybaric melting and mixing model that reproduced the combined trace element and long-lived isotope data for Iceland. The model mixed the accumulated melts from the depleted mantle and a recycled E-MORB crust at every depth in the melting region. Because of the highly incompatible nature of the U-series nuclides, the disequilibria for pure peridotitic or pyroxenitic sources calculated using dynamic melting, only change significantly during the initial stages of melting, that is extents of melting less than 3% (Figs. 10 and 11). Consequently, the effect of melting and mixing of a pyroxenite and a peridotite component and extraction of the mixed melts from various depths on the U-series disequilibria is small. As a result, the U-series disequilibria and highly incompatible trace element ratios of Icelandic lavas can be modelled by binary mixing (Figs. 10 and 11).

The variability of U-series disequilibria within the WV group can be explained by mixing of melts from a depleted peridotite with melts from an enriched E-MORB component characterised by high melt productivity and low D_U/D_{Th} (Fig. 10). The combined trace element, Hf isotope composition and U-series data for Theistareykir and WV samples is also broadly matched by mixing melts from the two components, supporting evidence for variable abundances of the mafic source component in the mantle beneath this part of Iceland (Fig. 11). The two WV Samples (WV21 and WV25) with higher U/Th and Nb/U but low (^{231}Pa/^{235}U), (^{230}Th/^{238}U) and Hf isotope ratios could result from melting a source containing more of the enriched component compared to samples with low Nb/U and high ^{231}Pa, ^{230}Th excesses and Hf ratios (WV31). Variability in ^{230}Th excesses for the Reykjanes Peninsula samples that erupted at similar distances from the plume centre (RP 5 and RP 6, Fig. 6), can similarly be explained by variable amounts of recycled material in the source, but at a lower mantle upwelling velocity compared to below the Western Volcanic Zone. Sample RP6 with the highest Nb/U within

the RP group for example, has the lowest (^{230}Th/^{238}U), supporting mixing with the E-MORB source with low D_U/D_{Th}. Using the model parameters in Table 2, predictions for the maximum abundance of the enriched component vary between ∼10% and up to 100% to explain the combined U-series and trace element compositions of WV25. The highly depleted WV31 and samples from Theistareykir in the Northern Rift Zone can be explained by melting of peridotite containing only small amounts of the enriched component (∼1%). Based on relationships between trace element and Nd and Hf isotope compositions, the maximum abundance of the enriched component in the source beneath the Western Volcanic zone was estimated to be 10% (Koornneef et al., 2012). The overestimates for the abundance of the enriched component are mainly due to parameters that involve the Th/U ratios and likely arise from uncertainties in the composition of the end-members.

Prytulak and Elliott (2009) investigated the relationship between melt productivity and the presence of pyroxenite in the mantle source beneath Pico, Azores, but found no apparent relation between source composition and the U-series disequilibria. The limited variability in ^{230}Th and ^{231}Pa excesses in Pico lavas were suggested to reflect melting of a peridotitic source alone and so a 'distillation' melting process that masks the effect of initial pyroxenite melting was required. For Iceland, the relationship between highly incompatible trace element ratios and ^{231}Pa and ^{230}Th excesses indicates that the pyroxenitic signature is preserved in the melt mixtures and that a melt–rock reaction as inferred by Prytulak and Elliott (2009) for the Azores is unlikely to have taken place beneath Iceland.

6. CONCLUSIONS

^{230}Th excesses in recent Icelandic lavas correlate with distance from the plume centre and the mean variation in U-series disequilibria can be explained by mantle upwelling velocities of ∼14 cm/yr at the plume axis to ∼4 cm/yr at the plume periphery. Both the absolute value and the range of inferred upwelling velocities are, however, model-sensitive. The comparatively few (^{231}Pa/^{235}U) data reported here do not substantiate the inferences from the (^{230}Th/^{238}U) data on the effect of the plume. More ^{231}Pa data on samples that are little influenced by source heterogeneity (e.g., low Nb/U, U/Th) or crustal processes (low SiO$_2$, high MgO) may, however, help resolve the significance and magnitude of buoyancy-related variations in upwelling velocity of the sub-Icelandic mantle.

Samples from the Western Rift Zone show that variability of the U-series disequilibria on a local scale is influenced by radioactive decay during melt transport, and/or variations in the mantle porosity rather than by local variations in mantle upwelling velocity in the sub-ridge melting region In addition, correlations of highly incompatible trace element ratios with (^{230}Th/^{238}U) and (^{231}Pa/^{235}U) on a local scale, however reveal that melts from an enriched pyroxenite component characterised by high melt productivity influence the U-series disequilibria significantly. Overall, our results demonstrate that information about the variability in regional mantle upwelling velocity can be extracted from U-series disequilibria, but that lithological heterogeneity affects the melting behaviour in MOR and OIB settings on a local scale. Detailed studies that apply combined U-series and trace element data on samples from confined areas on ocean islands, such as the Western Volcanic Zone in Iceland, are likely to further reveal the influence of source heterogeneity and would help to constrain the composition, spatial distribution and melting behaviour of enriched source components. The data presented here, for example, suggests that the enriched component is characterised by high melt productivity, but has low bulk D_U/D_{Th}. Even though low bulk D_U/D_{Th}'s are consistent with experimental melting of pyroxenite (Pertermann et al., 2004), the available data to support this hypothesis is scarce. Further experiments on U–Th partitioning during melting of mafic lithologies would thus be useful.

REFERENCES

Asimow P. D., Hirschmann M. M. and Stolper E. M. (1997) An analysis of variations in isentropic melt productivity. *Philos. Trans. R. Soc. Math. Phys. Eng. Sci.* **355**, 255–281.

Asimow P. D., Hirschmann M. M. and Stolper E. M. (2001) Calculation of peridotite partial melting from thermodynamic models of minerals and melts, IV. Adiabatic decompression and the composition and mean properties of mid-ocean ridge basalts. *J. Petrol.* **42**, 963–998.

Beattie P. (1993a) The generation of uranium series disequilibria by partial melting of spinel peridotite – constraints from partitioning studies. *Earth Planet. Sci. Lett.* **117**, 379–391.

Beattie P. (1993b) Uranium thorium disequilibria and partitioning on melting of garnet peridotite. *Nature* **363**, 63–65.

Blundy J. and Wood B. (2003) Mineral-melt partitioning of uranium, thorium and their daughters. *Rev. Mineral. Geochem.* **52**, 59–123.

Bourdon B. and Sims K.W.W. (2003) U-series constraints on intraplate basaltic magmatism. In: *Uranium-Series Geochemistry* (B. H. Bourdon, G. M. Lundstrom, C. C. Turner, (eds.), Reviews in Mineralogy and Geochemistry 52. pp. 215–254.

Bourdon B., Langmuir C. H. and Zindler A. (1996) Ridge-hotspot interaction along the Mid-Atlantic Ridge between 37°30′ and 40°30′N: the U–Th disequilibrium evidence. *Earth Planet. Sci. Lett.* **142**, 175–189.

Bourdon B., Joron J.-L., Claude-Ivanaj C. and Allegre C. J. (1998) U–Th–Pa–Ra systematics for the Grande Comore volcanics: melting processes in an upwelling plume. *Earth Planet. Sci. Lett.* **164**, 119–133.

Bourdon B., Turner S. P. and Ribe N. M. (2005) Partial melting and upwelling rates beneath the Azores from a U-series isotope perspective. *Earth Planet. Sci. Lett.* **239**, 42–56.

Bourdon B., Ribe N. M., Stracke A., Saal A. E. and Turner S. P. (2006) Insights into the dynamics of mantle plumes from uranium-series geochemistry. *Nature* **444**, 713–717.

Bourdon B. and Van Orman J. A. (2009) Melting of enriched mantle beneath Pitcairn seamounts: unusual U–Th–Ra systematics provide insights into melt extraction processes. *Earth Planet. Sci. Lett.* **277**, 474–481.

Braun M. G. and Sohn R. A. (2003) Melt migration in plume-ridge systems. *Earth Planet. Sci. Lett.* **213**, 417–430.

Chabaux F., Othman D. B. and Birck J. L. (1994) A new Ra–Ba chromatographic separation and its application to Ra mass-spectrometric measurement in volcanic rocks. *Chem. Geol.* **114**, 191–197.

Chauvel C. and Hémond C. (2000) Melting of a complete section of recycled oceanic crust: trace element and Pb isotopic evidence from Iceland. *Geochem. Geophys. Geosyst.* **1**, Q1234, http://dx.doi.org/10.1029/1999GC000002.

Chekol T. A., Kobayashi K., Yokoyama T., Sakaguchi C. and Nakamura E. (2011) Timescales of magma differentiation from basalt to andesite beneath Hekla Volcano, Iceland: constraints from U-series disequilibria in lavas from the last quarter-millennium flows. *Geochim. Cosmochim. Acta* **75**, 256–283.

Chen J. H., Lawrence Edwards. R. and Wasserburg G. J. (1986) ^{238}U, ^{234}U and ^{232}Th in seawater. *Earth Planet. Sci. Lett.* **80**, 241–251.

Claude-Ivanaj C., Bourdon B. and Allègre C. J. (1998) Ra–Th–Sr isotope systematics in Grande Comore Island: a case study of plume–lithosphere interaction. *Earth Planet. Sci. Lett.* **164**, 99–117.

Cohen A. and O'Nions S. R. K. (1993) Melting rates beneath Hawaii: evidence from uranium series isotopes in recent lavas. *Earth Planet. Sci. Lett.* **120**, 169–175.

Condomines M., Morand P., Allegre C. J. and Sigvaldason G. (1981) ^{230}Th–^{238}U disequilibria in historical lavas from Iceland. *Earth Planet. Sci. Lett.* **55**, 393–406.

Elkins L. J., Gaetani G. A. and Sims K. W. W. (2008) Partitioning of U and Th during garnet pyroxenite partial melting: constraints on the source of alkaline ocean island basalts. *Earth Planet. Sci. Lett.* **265**, 270–286.

Elliott T. R., Hawkesworth C. J. and Gronvold K. (1991) Dynamic melting of the Iceland plume. *Nature* **351**, 201–206.

Elliott T., Spiegelman M., Heinrich D. H. and Karl K. T. (2003) *Melt migration in oceanic crustal production: a U-series perspective, Treatise on Geochemistry*. Pergamon, Oxford, pp. 465–510.

Fabbrizio A., Schmidt M. W., Gunther D. and Eikenberg J. (2009) Experimental determination of Ra mineral/melt partitioning for feldspars and Ra-226-disequilibrium crystallization ages of plagioclase and alkali-feldspar. *Earth Planet. Sci. Lett.* **280**, 137–148.

Gee M. A. M., Taylor R. N., Thirlwall M. F. and Murton B. J. (1998) Glacioisostacy controls chemical and isotopic characteristics of tholeiites from the Reykjanes peninsula, SW Iceland. *Earth Planet. Sci. Lett.* **164**, 1–5.

Goldstein S. J., Murrell M. T. and Williams R. W. (1993) ^{231}Pa and ^{230}Th chronology of mid-ocean ridge basalts. *Earth Planet. Sci. Lett.* **115**, 151–159.

Hanan B. B., Blichert-Toft J., Kingsley R. and Schilling J. G. (2000) Depleted Iceland mantle plume geochemical signature: artifact of multicomponent mixing? *Geochem. Geophys. Geosyst.* **1**, Q1003, http://dx.doi.org/10.1029/1999GC000009.

Hauri E. H., Wagner T. P. and Grove T. L. (1994) Experimental and natural partitioning of Th, U, Pb and other trace-elements between garnet, clinopyroxene and basaltic melts. *Chem. Geol.* **117**, 149–166.

Hirschmann M. M. and Stolper E. M. (1996) A possible role for garnet pyroxenite in the origin of the "garnet signature" in MORB. *Contrib. Mineral. Petrol.* **124**, 185–208.

Hirschmann M. M., Ghiorso M. S., Wasylenki L. E., Asimow P. D. and Stolper E. M. (1998) Calculation of peridotite partial melting from thermodynamic models of minerals and melts. I. Review of methods and comparison with experiments. *J. Petrol.* **39**, 1091–1115.

Hirschmann M. M., Asimow P. D., Ghiorso M. S. and Stolper E. M. (1999a) Calculation of peridotite partial melting from thermodynamic models of minerals and melts. III. Controls on isobaric melt production and the effect of water on melt production. *J. Petrol.* **40**, 831–851.

Hirschmann M. M., Ghiorso M. S. and Stolper E. M. (1999b) Calculation of peridotite partial melting from thermodynamic models of minerals and melts. II. Isobaric variations in melts near the solidus and owing to variable source composition. *J. Petrol.* **40**, 297–313.

Ito G., Lin J. and Gable C. W. (1996) Dynamics of mantle flow and melting at a ridge-centered hotspot: Iceland and the Mid-Atlantic Ridge. *Earth Planet. Sci. Lett.* **144**, 53–74.

Ito G., Shen Y., Hirth G. and Wolfe C. J. (1999) Mantle flow, melting, and dehydration of the Iceland mantle plume. *Earth Planet. Sci. Lett.* **165**, 81–96.

Iwamori H. (1993) A model for disequilibrium mantle melting incorporating melt transport by porous and channel flows. *Nature* **366**, 734–737.

Iwamori H. (1994) ^{238}U–^{230}Th–^{226}Ra- and ^{235}U–^{231}Pa disequilibria produced by mantle melting with porous and channel flows. *Earth Planet. Sci. Lett.* **125**, 1–16.

Jull M. and McKenzie D. (1996) The effect of deglaciation on mantle melting beneath Iceland. *J. Geophys. Res. Solid Earth* **101**, 21815–21828.

Jull M., Kelemen P. B. and Sims K. (2002) Consequences of diffuse and channelled porous melt migration on uranium series disequilibria. *Geochim. Cosmochim. Acta* **66**, 4133–4148.

Katz R. F. (2008) Magma dynamics with the enthalpy method: benchmark solutions and magmatic focusing at mid-ocean ridges. *J. Petrol.* **49**, 2099–2121.

Klemme S., Blundy J. D. and Wood B. J. (2002) Experimental constraints on major and trace element partitioning during partial melting of eclogite. *Geochim. Cosmochim. Acta* **66**, 3109–3123.

Kogiso T., Hirschmann M. M. and Pertermann M. (2004) High-pressure partial melting of mafic lithologies in the mantle. *J. Petrol.* **45**, 2407–2422.

Kokfelt T. F., Hoernle K. and Hauff F. (2003) Upwelling and melting of the Iceland plume from radial variation of ^{238}U–^{230}Th disequilibria in postglacial volcanic rocks. *Earth Planet. Sci. Lett.* **214**, 167–186.

Kokfelt T. F., Hoernle K., Hauff F., Fiebig J., Werner R. and Garbe-Schoenberg D. (2006) Combined traced element and Pb–Nd–Sr–O isotope evidence for recycled oceanic crust (upper and lower) in the Iceland mantle plume. *J. Petrol.* **47**, 1705–1749.

Kokfelt T. F., Hoernle K., Lundstrom C., Hauff F. and van den Bogaard C. (2009) Time-scales for magmatic differentiation at the Snaefellsjokull central volcano, western Iceland: constraints from U–Th–Pa–Ra disequilibria in post-glacial lavas. *Geochim. Cosmochim. Acta* **73**, 1120–1144.

Koornneef J. M., Stracke A., Aciego S., Reubi O. and Bourdon B. (2010) A new method for U-Th-Pa-Ra separation and accurate measurement of ^{234}U–^{230}Th–^{231}Pa–^{226}Ra disequilibria in volcanic rocks by MC-ICPMS. *Chem. Geol.* **277**, 30–41.

Koornneef J. M., Stracke A., Bourdon B., Meier M. A., Jochum K. P., Stoll B. and Grönvold K. (2012) Melting of a two-component source beneath Iceland. *J. Petrol.* **53**, 127–157.

Kuritani T., Yokoyama T., Kitagawa H., Kobayashi K. and Nakamura E. (2011) Geochemical evolution of historical lavas from Askja Volcano, Iceland: implications for mechanisms and timescales of magmatic differentiation. *Geochim. Cosmochim. Acta* **75**, 570–587.

LaTourrette T. Z. and Burnett D. S. (1992) Experimental-determination of U-partitioning and Th-partitioning between clinopyroxene and natural and synthetic basaltic liquid. *Earth Planet. Sci. Lett.* **110**, 227–244.

LaTourrette T. Z., Kennedy A. K. and Wasserburg G. J. (1993) Thorium–uranium fractionation by garnet – evidence for a deep source and rapid rise of oceanic basalts. *Science* **261**, 739–742.

Lundstrom C. (2001) Models of U-series disequilibria generation in MORB: the effects of two scales of melt porosity. *Phys. Earth Planet. Inter.* **121**, 189–204.

Lundstrom C. C., Gill J., Williams Q. and Perfit M. R. (1995) Mantle melting and basalt extraction by equilibrium porous flow. *Science* **270**, 1958–1961.

Lundstrom C. C., Williams Q. and Gill J. B. (1998) Investigating solid mantle upwelling rates beneath mid-ocean ridges using U-series disequilibria, 1: a global approach. *Earth Planet. Sci. Lett.* **157**, 151–165.

Lundstrom C. C., Sampson D. E., Perfit M. R., Gill J. and Williams Q. (1999) Insights into mid-ocean ridge basalt petrogenesis: U-series disequilibria from the Siqueiros Transform, Lamont Seamounts, and East Pacific Rise. *J. Geophys. Res. Solid Earth* **104**, 13035–13048.

Lundstrom C. C., Gill J. and Williams Q. (2000) A geochemically consistent hypothesis for MORB generation. *Chem. Geol.* **162**, 105–126.

Lundstrom C. C., Hoernle K. and Gill J. (2003) U-series disequilibria in volcanic rocks from the Canary Islands: plume versus lithospheric melting. *Geochim. Cosmochim. Acta* **67**, 4153–4177.

Maclennan J. (2008a) Concurrent mixing and cooling of melts under Iceland. *J. Petrol.* **49**, 1931–1953.

Maclennan J. (2008b) Lead isotope variability in olivine-hosted melt inclusions from Iceland. *Geochim. Cosmochim. Acta* **72**, 4159–4176.

Maclennan J., McKenzie D. and Gronvold K. (2001) Plume-driven upwelling under central Iceland. *Earth Planet. Sci. Lett.* **194**, 67–82.

Maclennan J., Jull M., McKenzie D., Slater L. and Gronvold K. (2002) The link between volcanism and deglaciation in Iceland. *Geochem. Geophys. Geosyst.* **3**, Q1062, http://dx.doi.org/10.1029/2001GC000282.

Maclennan J., McKenzie D., Gronvold K., Shimizu N., Eiler J. M. and Kitchen N. (2003) Melt mixing and crystallization under Theistareykir, northeast Iceland. *Geochem. Geophys. Geosyst.* **4**, Q8624, http://dx.doi.org/10.1029/2003gc000558.

Maclennan J., McKenzie D., Hilton F., Gronvold K. and Shimizu N. (2007) Geochemical variability in a single flow from northern Iceland. *J. Geophys. Res. Solid Earth* **108**, http://dx.doi.org/10.1029/2000JB000142.

McDade P., Blundy J. D. and Wood B. J. (2003a) Trace element partitioning between mantle wedge peridotite and hydrous MgO-rich melt. *Am. Mineral.* **88**, 1825–1831.

McDade P., Blundy J. D. and Wood B. J. (2003b) Trace element partitioning on the Tinaquillo Lherzolite solidus at 1.5 GPa. *Phys. Earth Planet. Inter.* **139**, 129–147.

McKenzie D. (1985) ^{230}Th–^{238}U disequilibrium and the melting processes beneath ridge axes. *Earth Planet. Sci. Lett.* **72**, 149–157.

McKenzie D. and Bickle M. J. (1988) The volume and composition of melt generated by extension of the lithosphere. *J. Petrol.* **29**, 625–679.

McKenzie D., Stracke A., Blichert-Toft J., Albarede F., Gronvold K. and O'Nions R. K. (2004) Source enrichment processes responsible for isotopic anomalies in oceanic island basalts. *Geochim. Cosmochim. Acta* **68**, 2699–2724.

Olson P., Schubert G. and Anderson C. (1993) Structure of axisymmetrical mantle plumes. *J. Geophys. Res.-Sol. Ea.* **98**, 6829–6844.

Peate D. W., Hawkesworth C. J., van Calsteren P. W., Taylor R. N. and Murton B. J. (2001) ^{238}U–^{230}Th constraints on mantle upwelling and plume-ridge interaction along the Reykjanes Ridge. *Earth Planet. Sci. Lett.* **187**, 259–272.

Peate D., Baker J., Jakobsson S., Waight T., Kent A., Grassineau N. and Skovgaard A. (2009) Historic magmatism on the Reykjanes Peninsula, Iceland: a snap-shot of melt generation at a ridge segment. *Contrib. Mineral. Petrol.* **157**, 359–382.

Peate D. W., Breddam K., Baker J. A., Kurz M. D., Barker A. K., Prestvik T., Grassineau N. and Skovgaard A. C. (2010) Compositional characteristics and spatial distribution of enriched Icelandic mantle components. *J. Petrol.*, egq025.

Pertermann M. and Hirschmann M. M. (2002) Trace-element partitioning between vacancy-rich eclogitic clinopyroxene and silicate melt. *Am. Mineral.* **87**, 1365–1376.

Pertermann M. and Hirschmann M. M. (2003) Partial melting experiments on a MORB-like pyroxenite between 2 and 3 GPa: constraints on the presence of pyroxenite in basalt source regions from solidus location and melting rate. *J. Geophys. Res. Solid Earth* **108**, 2125, http://dx.doi.org/10.1029/2000JB000118.

Pertermann M., Hirschmann M. M., Hametner K., Gunther D. and Schmidt M. W. (2004) Experimental determination of trace element partitioning between garnet and silica-rich liquid during anhydrous partial melting of MORB-like eclogite. *Geochem. Geophys. Geosyst.* **5**, Q05A01. http://dx.doi.org/10.1029/2003gc000638.

Phipps Morgan J. (2001) Thermodynamics of pressure release melting of a veined plum pudding mantle. *Geochem. Geophys. Geosyst.* **2**.

Pickett D. A. and Murrell M. T. (1997) Observations of ^{231}Pa/^{235}U disequilibrium in volcanic rocks. *Earth Planet. Sci. Lett.* **148**, 259–271.

Pietruszka A. J., Hauri E. H. and Blichert-Toft J. (2009) Crustal contamination of mantle-derived magmas within Piton de la Fournaise Volcano, Runion Island. *J. Petrol.* **50**, 661–684.

Prytulak J. and Elliott T. (2007) TiO$_2$ enrichment in ocean island basalts. *Earth Planet. Sci. Lett.* **263**, 388–403.

Prytulak J. and Elliott T. (2009) Determining melt productivity of mantle sources from ^{238}U–^{230}Th- and ^{235}U–^{231}Pa disequilibria; an example from Pico Island, Azores. *Geochim. Cosmochim. Acta* **73**, 2103–2122.

Reubi O., Bourdon B., Dungan M. A., Koornneef J. M., Sellés D., Langmuir C. H. and Aciego S. (2011) Assimilation of the plutonic roots of the Andean arc controls variations in U-series disequilibria at Volcan Llaima, Chile. *Earth Planet. Sci. Lett.* **303**, 37–47.

Ribe N. M., Christensen U. R. and Theissing J. (1995) The dynamics of plume-ridge interaction.1. Ridge-centered plumes. *Earth Planet. Sci. Lett.* **134**, 155–168.

Ruedas T., Schmeling H., Marquart G., Kreutzmann A. and Junge A. (2004) Temperature and melting of a ridge-centred plume with application to Iceland. Part I: Dynamics and crust production. *Geophys. J. Int.* **158**, 729–743.

Russo C. J., Rubin K. H. and Graham D. W. (2009) Mantle melting and magma supply to the Southeast Indian Ridge: the

roles of lithology and melting conditions from U-series disequilibria. *Earth Planet. Sci. Lett.* **278**, 55–66.

Salters V. J. M. and Longhi J. (1999) Trace element partitioning during the initial stages of melting beneath mid-ocean ridges. *Earth Planet. Sci. Lett.* **166**, 15–30.

Salters V. J. M., Longhi J. E. and Bizimis M. (2002) Near mantle solidus trace element partitioning at pressures up to 3.4 GPa. *Geochem. Geophys. Geosyst.* **3**, Q1038, http://dx.doi.org/1010.1029/2001gc000148.

Shorttle O., Maclennan J. and Jones S. M. (2011) Control of the symmetry of plume-ridge interaction by spreading ridge geometry. *Geochem. Geophys. Geosyst.* **11**, Q0AC05. http://dx.doi.org/10.1029/2009gc002986.

Sigmarsson O., Hemond C., Condomines M., Fourcade S. and Oskarsson N. (1991) Origin of silicic magma in Iceland revealed by Th isotopes. *Geology* **19**, 621–624.

Sigmarsson O., Condomines M. and Fourcade S. (1992) Mantle and crustal contribution in the genesis of recent basalts from off-rift zones in Iceland: constraints from Th, Sr and O isotopes. *Earth Planet. Sci. Lett.* **110**, 149–162.

Sims K. W. W. S., DePaolo Donald J., Murrell Michael T., Scott Baldridge W., Goldstein Steven J. and Clague David A. (1995) Mechanisms of magma generation beneath Hawaii and Mid-Ocean Ridges: uranium/thorium and samarium/neodymium isotopic evidence. *Science* **267**, 508–512.

Sims K. W. W., DePaolo D. J., Murrell M. T., Baldridge W. S., Goldstein S., Clague D. and Jull M. (1999) Porosity of the melting zone and variations in the solid mantle upwelling rate beneath Hawaii: inferences from $^{238}U–^{230}Th–^{226}Ra$ and $^{235}U–^{231}Pa$ disequilibria. *Geochim. Cosmochim. Acta* **63**, 4119–4138.

Sims K. W. W., Goldstein S. J., Blichert-Toft J., Perfit M. R., Kelemen P., Fornari D. J., Michael P., Murrell M. T., Hart S. R., DePaolo D. J., Layne G., Ball L., Jull M. and Bender J. (2002) Chemical and isotopic constraints on the generation and transport of magma beneath the East Pacific Rise. *Geochim. Cosmochim. Acta* **66**, 3481–3504.

Sinton J., Grönvold K. and Sæmundsson K. (2005) Postglacial eruptive history of the Western Volcanic Zone, Iceland. *Geochem. Geophys. Geosyst.* **6**, Q12009, http://dx.doi.org/10.11029/12005GC001021.

Skovgaard A. C., Storey M., Baker J., Blusztajn J. and Hart S. R. (2001) Osmium–oxygen isotopic evidence for a recycled and strongly depleted component in the Iceland mantle plume. *Earth Planet. Sci. Lett.* **194**, 259–275.

Slater L., McKenzie D. A. N., Gronvold K. and Shimizu N. (2001) Melt generation and movement beneath Theistareykir, NE Iceland. *J. Petrol.* **42**, 321–354.

Spiegelman M. and Elliott T. (1993) Consequences of melt transport for uranium series disequilibrium in young lavas. *Earth Planet. Sci. Lett.* **118**, 1–20.

Stolper E. and Asimow P. (2007) Insights into mantle melting from graphical analysis of one-component systems. *Am. J. Sci.* **307**, 1051–1139.

Stracke A. and Bourdon B. (2009) The importance of melt extraction for tracing mantle heterogeneity. *Geochim. Cosmochim. Acta* **73**, 218–238.

Stracke A., Salters V. J. M. and Sims K. W. W. (1999) Assessing the presence of garnet–pyroxenite in the mantle sources of basalts through combined hafnium–neodymium–thorium isotope systematics. *Geochem. Geophys. Geosyst.* **1**, Q1006, http://dx.doi.org/10.1029/1999GC000013.

Stracke A., Zindler A., Salters V. J. M., McKenzie D. and Grönvold K. (2003a) The dynamics of melting beneath Theistareykir, northern Iceland. *Geochem. Geophys. Geosyst.* **4**, Q8513, http://dx.doi.org/10.1029/2002GC000347.

Stracke A., Zindler A., Salters V. J. M., McKenzie D., Blichert-Toft J., Albarede F. and Gronvold K. (2003b) Theistareykir revisited. *Geochem. Geophys. Geosyst.* **4**, Q8507, http://dx.doi.org/10.1029/2001GC000201.

Stracke A., Bourdon B. and McKenzie D. (2006) Melt extraction in the Earth's mantle: constraints from U–Th–Pa–Ra studies in oceanic basalts. *Earth Planet. Sci. Lett.* **244**, 97–112.

Sturm M. E., Goldstein S. J., Klein E. M., Karson J. A. and Murrell M. T. (2000) Uranium-series age constraints on lavas from the axial valley of the Mid-Atlantic Ridge. *MARK area. Earth Planet. Sci. Lett.* **181**, 61–70.

Turner S., Hawkesworth C., Rogers N. and King P. (1997) U–Th isotope disequilibria and ocean island basalt generation in the Azores. *Chem. Geol.* **139**, 145–164.

Turner S., Beier C., Niu Y. L. and Cook C. (2011) U–Th–Ra disequilibria and the extent of off-axis volcanism across the East Pacific Rise at 9 degrees 30′N, 10 degrees 30′N, and 11 degrees 20′N. *Geochem. Geophys. Geosyst.* **12**, Q0ac12, http://dx.doi.org/10.1029/2010gc003403.

Widom E., Schmincke H. U. and Gill J. B. (1992) Processes and timescales in the evolution of a chemically zoned trachyte – Fogo-a, Sao-Miguel, Azores. *Contrib. Mineral. Petrol.* **111**, 311–328.

Williams R. W. and Gill J. B. (1989) Effects of partial melting on the uranium decay series. *Geochim. Cosmochim. Acta* **53**, 1607–1619.

Wood D. A. (1981) Partial melting models for the petrogenesis of Reykjanes Peninsula Basalts, Iceland – implications for the use of trace-elements and strontium and neodymium isotope ratios to record inhomogeneities in the upper mantle. *Earth Planet. Sci. Lett.* **52**, 183–190.

Wood B. J. and Blundy J. D. (1997) A predictive model for rare earth element partitioning between clinopyroxene and anhydrous silicate melt. *Contrib. Mineral. Petrol.* **129**, 166–181.

Wood B. J., Blundy J. D. and Robinson J. A. C. (1999) The role of clinopyroxene in generating U-series disequilibrium during mantle melting. *Geochim. Cosmochim. Acta* **63**, 1613–1620.

Zhu W., Gaetani G. A., Fusseis F., Montési L. G. J. and De Carlo F. (2011) Microtomography of partially molten rocks: three-dimensional melt distribution in mantle peridotite. *Science* **332**, 88–91.